Leg compliance is required to explain the ground reaction force patterns and speed ranges in different gaits

Ali Tehrani Safa[1,a], Tirthabir Biswas[2,3,a], Arun Ramakrishnan[4], Vikas Bhandawat[1*]

September 7, 2024

[a]equal authors

[1]School of Biomedical Engineering, Science and Health Systems
Drexel University
Philadelphia, PA 19104, USA.

[2]Department of Neurobiology
Northwestern University
Evanston, IL 60208, USA.

[3]Janelia Research Campus
Howard Hughes Medical Institute
Ashburn, VA 20147, USA.

[4]College of Nursing and Health Professionals
Drexel University
Philadelphia, PA 19104, USA.

Abstract

Two simple models – vaulting over stiff legs and rebounding over compliant legs – are employed to describe the mechanics of legged locomotion. It is agreed that compliant legs are necessary for describing running and that legs are compliant while walking. Despite this agreement, stiff legs continue to be employed to model walking. Here, we show that leg compliance is necessary to model walking and, in the process, identify the principles that underpin two important features of legged locomotion: First, at the same speed, step length, and stance duration, multiple gaits that differ in the number of leg contraction cycles are possible. Among them, humans and other animals choose a gait with M-shaped vertical ground reaction forces because it is energetically favored. Second, the transition from walking to running occurs because of the inability to redirect the vertical component of the velocity during the double stance phase. Additionally, we also examine the limits of double spring-loaded pendulum (DSLIP) as a quantitative model for locomotion, and conclude that DSLIP is limited as a model for walking. However, insights gleaned from the analytical treatment of DSLIP are general and will inform the construction of more accurate models of walking.

*Author for correspondence - vb468@drexel.edu

1 Introduction

Understanding the movement of the center of mass (CoM) and the forces exerted on the CoM during locomotion is important because the behavior of the CoM describes the overall interaction between the animal and the environment during locomotion. The CoM movement and the forces exerted on them follow relatively simple patterns conserved across animals, suggesting that the overall animal-substrate interactions and, therefore, the underlying mechanical principles are simple and general (Blickhan, 1989; Geyer et al., 2006). The best example of the generality of mechanical principles is observed during running: Irrespective of the size of the animal, and the number of legs it uses, during running, the CoM reaches its minimum height at mid-stance and the vertical ground reaction force (vGRF) has an inverted "U"-shaped profile with a midstance maximum. This profile is well-explained by the spring-loaded inverted pendulum (SLIP), in which the mass of the animal is concentrated at a point. This point mass is supported by a massless spring (Blickhan, 1989; McMahon and Cheng, 1990; Blickhan and Full, 1993; Ahn et al., 2004; Daley et al., 2007; Nishikawa et al., 2007; Schmitt, 1999). The success of SLIP at modeling running shows that a body supported by a compliant leg is a good model for running – or locomotion at high speeds.

Unlike running, it is unclear whether leg compliance is important for walking – the gait used at low speeds. Initially, the inverted pendulum (IP) model, which uses a non-compliant or rigid leg, was used to model walking (Griffin et al., 2004; Usherwood, 2005; Buczek et al., 2006). The IP model successfully models the energetics of walking (Kuo, 2001; Donelan et al., 2002; Kuo, 2002; Kuo et al., 2005) explaining correctly the exchange of kinetic and potential energy during walking: During the first half of the stance phase, the speed of the CoM decreases as the height of the CoM increases. The increase in potential energy is reconverted into kinetic energy during the second half of the stance phase.

With modifications, IP can also model the work done during velocity redirection between steps which is important for estimating the energy cost of walking. During human walking, the CoM velocity vector is directed downwards at the end of the step and must be redirected upwards before the next step (Kuo, 2001; Adamczyk and Kuo, 2009; Donelan et al., 2002). In the IP model, velocity redirection occurs instantaneously, therefore, the work performed during the transition cannot be estimated. Regardless, many trends for work done during walking can be explained by distributing the force impulse in IP over a finite period of time; these modifications, however, are entirely *ad hoc*. Another, perhaps more fundamental, limitation of the IP model is that it cannot model the double-humped or M-shaped vertical GRF (vGRF) during walking. This limitation has been addressed in many ways: by modeling non-impulsive impact forces at the beginning and end of each step, and by using a telescoping actuator with bounds on impact forces (Srinivasan and Ruina, 2006; Srinivasan, 2011). However, the model that produces the most naturalistic force profiles assumes a linear relation between force and leg length, implying that a linear spring is likely necessary to model GRF during walking.

The limitation of IP model in producing appropriate forces, the fact that although IP correctly predicts the mid-stance maximum in the height of the CoM, the actual CoM height at mid-stance is lower, and the recent realization that legs are compliant during walking (Lee and Farley, 1998; Buczek et al., 2006) led to the development of the double SLIP (DSLIP) model, in which each leg of a biped is modeled as a spring (Figure 1A). DSLIP extends SLIP with a double stance phase during which the CoM is supported by two "springy" legs (Geyer et al., 2006; Rummel et al., 2010). DSLIP can produce the M-shaped GRFs observed during human walking by providing a smooth velocity redirection during the double stance phase. It also produces trajectories with mid-stance heights that are lower than IP and more in accordance with experimental data. While DSLIP is an attractive model, there are several issues regarding DSLIP as a model for locomotion. The first issue is whether DSLIP can explain the choice of gait. Although it is clear that DSLIP is versatile, and all the major gaits observed during bipedal walking can emerge from the DSLIP model (Gan et al., 2018), it is unclear whether the range of speed over which a gait is observed in DSLIP matches

the range of speeds observed in animals. In humans, for example, walking is the dominant mode of transport over a large range of speeds and is characterized by an M-shaped vertical ground reaction force (vGRF). DSLIP finds stable gaits with M-shaped GRF for only a limited range of speeds (Geyer et al., 2006; Lipfert et al., 2012). The reasons for this limited range of speed supported by DSLIP are not understood. Similarly, although humans walk over a wide range of speeds, they do transition to faster gaits like running at speeds much lower than arguments involving centrifugal forces and slipping suggests. Thus, evaluating whether the DSLIP model can explain why M-shaped GRFs are prevalent, and what underlies the transition from M-shaped GRFs to other gaits will provide insights into the role of compliance in walking.

A second issue is how well DSLIP models the kinematics and mechanics of human walking. This question has not been evaluated rigorously. In studies in which DSLIP is compared to experimental data, it predicts within-step variations in CoM height and ground reaction forces (GRFs) (Lipfert et al., 2012; Hubel and Usherwood, 2015) that are larger than those observed experimentally. A larger issue is how a successful model is defined. Most studies focus on a single aspect of locomotion such as GRFs. Considering GRFs, CoM kinematics, and real non-dimensionalized time (and not normalized time) at the same time is crucial because the CoM height, H, along with the gravitational acceleration constant, $g \approx 9.8$ m/s^2, determines the natural timescale of the system $\sqrt{\frac{R_{nat}}{g}}$, where, $R_{nat} \approx H$, is the natural spring length. A successful model must produce realistic GRFs within the constraints of experimentally observed CoM kinematics and stance duration. These three constraints are rarely satisfied (Maus et al., 2010; Lipfert et al., 2012; Maus et al., 2015) simultaneously in most studies of locomotion, leaving the problem under-constrained. A previous study took this approach to model the single support phase of human walking (Antoniak et al., 2019).

These issues raise the question of whether adding compliance to the leg is necessary for modeling human walking. In this study, we show that adding leg compliance through the DSLIP model allows the modeling of fundamental features of locomotion, which would not be possible without it. During locomotion, the radial and angular motions of the CoM must be synchronized. Leg compliance provides a natural mechanistic basis for understanding the implications of this synchronization. We show that leg compliance explains the gaits observed at a given speed and how they relate to different oscillatory modes of the spring. We further argue that the *normal* gait with the characteristic "M"-shaped GRF is preferred because it is energetically efficient. We also show that it is difficult to walk using this normal gait at high speeds because achieving the necessary velocity redirection in the vertical direction is difficult. While DSLIP seems particularly limited in its ability to produce M-shaped GRFs, it enabled us to understand the fundamental reason behind why humans (and other animals) transition to faster gaits at size-specific speeds (Froude number $\equiv$ (speed)$^2/gR_{nat}$) that are significantly lower than 1, the approximate transition speed predicted by IP. We argue that once compliance is added, (which is certainly present during walking) speeds at which walking with a normal gait can occur are limited by the inability to perform large velocity redirections. We also show that linear springs are fundamentally limited and cannot support normal walking above a Froude number ~ 0.25. Our analysis thus strongly suggests that while a spring with a constant stiffness cannot model human walking except for a narrow range of speeds, a compliant leg is necessary to understand fundamental constraints and optimization criteria that describe walking dynamics. Hence, DSLIP is a far superior starting point for more complex locomotion models than without leg compliance.

2 Results

Throughout the manuscript, we employ the DSLIP model (Figure 1A) in which both legs are modeled as massless springs to gain insight into the role of compliance in walking. Each leg has the same stiffness, K_s, and natural length, R_{nat}. The dynamics of the single stance phase are the same as SLIP; the swing dynamics are not modeled. The single stance phase transitions to a double stance

phase when the distance between the CoM and the future footstep equals the spring's natural length, and we assume that the swing leg has "touched down". The step length, L, between two consecutive foot positions is another parameter. We will focus on symmetric gaits so that the lift-off of the receding leg and the touch-down of the leading leg occur at time points given by time-reversal symmetry about the mid-step time. All variables in their dimensional and dimensionless forms are enumerated in the table below.

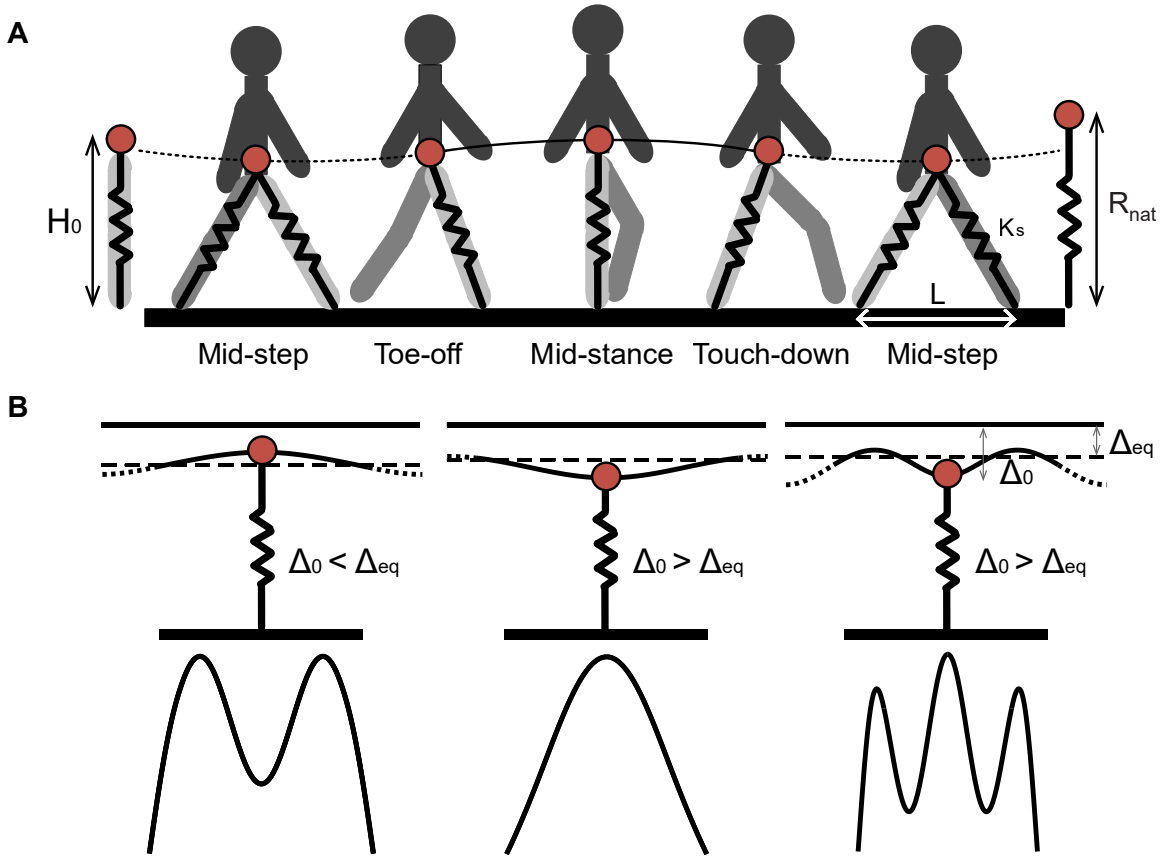

Figure 1. The position of the CoM at mid-stance in relation to the equilibrium point of the spring-mass system determines the GRF profile. A. Gait cycle for normal human walking showing the mid-stance maximum in height and a mid-step minimum in height. The DSLIP model is overlayed on the step cycle. Solid lines and dotted lines represent single and double stance phases respectively. **B.** The top row shows the position of the CoM at mid-stance in relation to the equilibrium position. During human walking (left), the CoM at mid-stance is above this equilibrium point; the resulting vGRF will be at its minimum and produce an M-shaped vGRF. In grounded running (middle), the CoM is at its minimum height below the equilibrium point resulting in the maximum spring contraction/force at mid-stance. Walking with multiple oscillations (right) can have either a maximum or minimum CoM height regarding the number of oscillations. Again with the same logic, the extremums of vGRF profile are defined based on the position of the CoM related to the equilibrium point.

2.1 Emergence of different walking gaits and their energetics

Different gaits are oscillatory modes of the DSLIP model

In previous work, it has already been shown that the DSLIP model can function in multiple

The model's parameters

Parameter	Symbol	Dimensionless form	Relation
Mass	M	N/A	N/A
Acceleration of gravity	g	N/A	N/A
Weight	W	N/A	W = Mg
Natural spring length	R_{nat}	N/A	N/A
Time	t	τ	$\tau = t\sqrt{\frac{g}{R_{nat}}}$
Single stance time	t_s	τ_s	$\tau_s = t_s\sqrt{\frac{g}{R_{nat}}}$
Double stance time	t_d	τ_d	$\tau_d = t_d\sqrt{\frac{g}{R_{nat}}}$
Spring stiffness	K_s	γ	$\gamma = \frac{K_s R_{nat}}{W}$
Step length	L	λ	$\lambda = \frac{L}{R_{nat}}$
Radial Coordinate	R	r	$r = \frac{R}{R_{nat}}$
Initial radial coordinate	R_0	r_0	$r_0 = \frac{R_0}{R_{nat}}$
Radial coordinate at equilibrium	R_{eq}	r_{eq}	$r_{eq} = 1$ - $\frac{1}{\gamma}$
Radial coordinate at transition	$R_\star$	$r_\star$	$r_\star = \frac{R_\star}{R_{nat}}$
Height of CoM	H	h	$h = \frac{H}{R_{nat}}$
Height of CoM at mid-stance	H_0	h_0	$h_0 = \frac{H_0}{R_{nat}}$
Spring contraction	Δ	δ	$\delta = 1 - r$
Initial spring contraction	Δ_0	δ_0	$\delta_0 = 1 - r_0$
Spring contraction at equilibrium	Δ_{eq}	δ_{eq}	$\delta_{eq} = \frac{1}{\gamma}$
Spring contraction at transition	$\Delta_\star$	$\delta_\star$	$\delta_\star = 1 - r_\star$
Angular coordinate	θ	θ	N/A
Angular coordinate at transition	$\theta_\star$	$\theta_\star$	N/A
Initial angular velocity	$\dot{\theta}_0$	Ω_0	$\Omega_0 = \dot{\theta}_0\sqrt{\frac{g}{R_{nat}}}$
Maximal Spring Energy	E	ϵ	$\epsilon = \frac{E}{MgR_{nat}} = \frac{1}{2}\gamma\delta_{\max}^2$
Oscillation frequency	N/A	ω	$\omega = \sqrt{\gamma}$
Oscillation phase	N/A	ϕ	$\phi = \omega t$
Oscillation phase at transition	N/A	$\phi_\star$	N/A
Horizontal displacement of the CoM	X_{com}	x	$x = \frac{X_{com}}{R_{nat}}$
Vertical displacement of the CoM	Y_{com}	y	$y = \frac{Y_{com}}{R_{nat}}$
Average CoM's speed	V_{com}	v	$v = \frac{V_{com}}{\sqrt{gR_{nat}}}$
Froude number	N/A	Fr	$Fr = (\frac{\lambda}{\tau_s+\tau_d})^2$
Horizontal velocity at transition	N/A	$v_{x_\star}$	$v_{x_\star} \approx (1-\delta_\star)\Omega_0\cos\theta_\star$
Vertical velocity at transition	N/A	$v_{y_\star}$	$v_{y_\star} \approx -(1-\delta_\star)\Omega_0\sin\theta_\star$
Vertical acceleration at transition	N/A	$a_{y_\star}$	$a_{y_\star} \approx \gamma\delta_\star\cos\theta_\star - 1$

modes (Geyer et al., 2006; Gan et al., 2018; Andrada et al., 2020; Ding et al., 2022; Mauersberger et al., 2022); these modes include common modes of animal locomotion. These different modes arise from different positions of the CoM in relation to the equilibrium length of the spring (Figure 1). To describe the different modes, instead of leg length, it is more convenient to introduce the spring compression, Δ, via $R = R_{nat} - \Delta$. Each mode is an oscillation around the fixed point,

$R = R_{eq} = R_{nat} - \Delta_{eq}$, of the spring-mass system given by the Δ where the spring force balances gravity, $\Delta_{eq} = Mg/K_s$, where M is the mass of the subject. Assuming symmetry, at mid-stance the radial coordinate and the height must be either at a maximum or a minimum. At the take-off point, the leg reaches its maximal length or the natural length, R_{nat}. Whether the mid-stance height is at a maximum or minimum is determined by the relationship between the compression at mid-stance, Δ_0, and Δ_{eq}: If $\Delta_0 > \Delta_{eq}$, the weight is larger than the spring force at mid-stance, the net vertical force points downwards, the second derivative of the height at mid-stance, $\ddot{H}_0$, is negative, and the CoM must go down, resulting in a maximum in height and leg length. Thereafter, it must undergo approximately an integral number of oscillations before take-off. Normal human walking with its mid-stance maximum in height is the most common gait of this kind with approximately a single radial oscillation between the mid-stance and take-off (Figure 1B, left).

In contrast, if the leg starts below the equilibrium, $\Delta_0 < \Delta_{eq}$, the spring force is larger than the weight, leading to an upward net vertical force, $\ddot{H}_0 > 0$, and therefore a minimum in height and leg length. The radial coordinate undergoes approximately half-integral oscillations before take-off, Figure 1B, middle. The lowest oscillatory mode with approximately half of an oscillation corresponds to the grounded running gait that is employed over a limited speed range in humans but over a large range of speed in some birds ((Andrada et al., 2013b, 2020; Davis et al., 2020). In Figure 1B, right, we also show gait patterns of this type with more than one vertical oscillation.

The possible gait patterns and the ranges over which they are found, when we have at most one oscillation, are summarized in Figure 2. We have used dimensionless quantities in Figure 2 that will be introduced shortly. As we just explained, the different modes of DSLIP depend on the height of the CoM, H_0, at midstance in relation to the equilibrium height R_{eq} which in turn depends on the angular speed at mid-stance, and K_s. However, due to the centrifugal force resulting from the angular motion, this transition occurs at a CoM height, H_0, that is slightly higher than the equilibrium height (see Appendix A for a detailed derivation). Due to the centrifugal force, apart from the normal walking mode, there is a small range of Δ_0 values for which the gait has a mid-stance maximum in height but not an M-shaped GRF. We refer to this gait as Inverted walking. Finally, there is a large range of values where grounded running, with a height minimum and inverted "U"-shaped vGRF maximum, is observed, consistent with theoretical work and the fact that many animals show grounded running (Andrada et al., 2013b; Blickhan et al., 2018; Andrada et al., 2020). The grounded running and inverted walking gaits are together referred to as inverted gaits as they both have an inverted "U"-shaped vGRF maximum, as opposed to the "M" shape observed in normal walking.

Gait parameter space

To evaluate the exact ranges we found limit cycle solutions. A priori, there are five dimensional parameters that control the evolution of a symmetric gait: stiffness and natural length of the leg spring, K_s and R_{nat}, respectively, the step length, L, and the height and angular velocity at mid-stance, H_0 and $\dot{\theta}_0$, respectively. Together, these five parameters completely specify a symmetric walking trajectory for CoM. We note that time-reversal symmetry requires that at mid-stance and mid-step, $\dot{H}$ must be zero, or the height must be at a maximum or minimum. Typically, as the CoM evolves and reaches mid-step, $\dot{H}$ will not be zero, a condition that is required for a symmetric gait cycle. Imposing $\dot{H} = 0$ at the mid-step, provides an additional constraint, leaving only four independent parameters among $\{K_s, R_{\text{nat}}, L, H_0, \dot{\theta}_0\}$ that now uniquely parametrizes limit cycles. To simplify the analysis further, we used dimensionless quantities (by setting $R_{\text{nat}} = 1$): the dimensionless angular speed and length contraction at the mid-stance, Ω_0 and δ_0, the dimensionless spring constant, γ, and relative step length, λ. Of these four, only three are independent due to the limit cycle requirement.

The range of speeds, expressed as Froude number, Fr, the square of the dimensionless average velocity (approximately equals ${\Omega_0}^2$), over which limit cycle walking is possible at a given λ is shown in Figure 3A. Limit cycles with M-shaped vGRF are found over the range of speeds over which

Gait	CoM height	GRFs	$\gamma\delta_0$ range
Normal walking	Max	Min	$0 < \gamma\delta_0 \leq 1 - \Omega_0^2$
Inverted walking	Max	Max	$1 - \Omega_0^2 < \gamma\delta_0 \leq 1$
Grounded running	Min	Max	$1 < \gamma\delta_0$

Figure 2. vGRFs and CoM trajectories for different gaits with at most a single contraction-expansion cycle between mid-stance and mid-step and the limits within which each is supposed to occur. The range over which different gaits are observed depends mostly on whether the spring is compressed more or less than the compression necessary to balance the gravitation force. The Ω_0^2 term compensates for the centripetal acceleration and will be small for most walking speeds.

humans typically walk. M-shaped vGRF is possible at low speeds with a DSLIP model but not at the highest speed observed during M-shaped human walking. That DSLIP cannot model M-shaped walking at the higher end of walking speeds is a well-known limitation of the DSLIP model (Geyer, 2005; Geyer et al., 2006; Lipfert et al., 2012; Mauersberger et al., 2022; Lin et al., 2023) that we will explore in the next section. Modes with higher oscillations are found only at low speeds (orange region in Figure 3A). as going through multiple oscillations takes time, increases stance duration, and decreases speed.

The range of speeds for which a single-humped vGRF (inverted gaits) was observed is more extensive than the M-shaped vGRF. At low speeds, both the M-shaped vGRF and the inverted force profiles are possible using different γ values. However, only the inverted force profile is possible at high Froude numbers. Part of this regime (green area) corresponds to grounded running. Consistent with grounded running observed in humans and other bipeds (Andrada et al., 2013b; Blickhan et al., 2018; Andrada et al., 2020; Davis et al., 2020), the spring constant decreases as the gait transitions from normal walking to grounded running.

Normal walking gait with "M"-shaped vGRF are preferred because they are energetically efficient

Why do humans choose M-shaped GRFs during walking despite other modes being accessible? A possible reason is that the normal gait is energetically most efficient. Although DSLIP itself is a conservative model, the spring compression modeled by DSLIP will require work that will be proportional to the energy stored in the SLIP spring. Thus one can use the maximum spring energy stored as a proxy for energy cost of transport during the given walking step. Now, the maximal stored energy is given by

$$\epsilon = \frac{1}{2}\gamma\delta_{\max}^2 \ . \tag{2.1}$$

The stored energy for a given walking speed, Ω_0, for the normal and inverted gaits can be estimated. For the normal gait, $\delta_{\max} \approx 2/\gamma - \delta_0$, while in the inverted gaits, $\delta_{\max} \approx \delta_0 > 1/\gamma$ (Figure 1). In

the normal gait, the minimum ϵ is achieved by choosing $\delta_0 \to 1/\gamma \Rightarrow \delta_{\max} \to 1/\gamma$, so that

$$\epsilon_{\text{min,normal}} \approx \frac{1}{2\gamma} \ . \tag{2.2}$$

Since $\delta_0 > 1/\gamma$ in the inverted gaits ϵ is minimized as $\delta_0 \to 1/\gamma$ as well. Note that for the normal gait $1/\gamma$ is the largest value of δ_0 , while for the inverted gait, it is the lowest.

$$\epsilon_{\text{min,inverted}} = \frac{1}{2}\gamma\delta_0^2 = \frac{1}{2\gamma} \ . \tag{2.3}$$

For a given speed, the expression for the minimum stored energy is the same for both gaits, and is inversely proportional to γ. Therefore, the gait with higher γ is preferred. That the normal gait is a high stiffness gait is observed in Figure 3A. The same can be inferred intuitively: The take-off angle, θ_{off}, does not change very much between different walking trajectories. Thus the time, $\theta_{\text{off}}/\Omega_0$, that a leg is on the ground stays approximately the same as long as the walking speed is the same. However, in this time, during normal walking the radial coordinate must oscillate once, while in the grounded running gait it only has to undergo half an oscillation. Since oscillation frequency goes as the square root of stiffness, γ, this means that the normal walking gait must have a larger stiffness, and is thus preferred over the inverted gaits.

To quantitatively test this idea, we evaluated the ϵ over the entire space where we have limit cycle solutions and ϵ was smaller for the normal gait compared to the inverted gaits (Figure 3B) for the same speed. Therefore, M-shaped vGRFs are preferable to grounded running because it minimizes energy. A similar argument, however, does suggest that multiple oscillatory modes would have even higher stiffness and, therefore, should be preferred over the normal gait. So why don't we observe these gaits more frequently? One reason is that each gait (except the grounded running gait) has a maximum attainable speed, and the higher the number of oscillations, the smaller this speed-bound. Another possible reason is that the higher oscillatory modes require a much larger stiffness, making them biologically undesirable. Within the preferred speed range of human walking, higher oscillatory modes are not available (or have very large stiffness), making the normal walking gait the most energy-efficient gait.

This analysis above ignores the energy used to propel the swing leg; approximate assessment of the energetics of the swing phase show that normal gait will be preferred. It has been previously proposed that the swing energy is $\propto \nu^4$, where $\nu = 1/(\tau_s)$ is the angular frequency of the swing leg, and τ_s is the dimensionless time for the single stance/swing phase (Kuo et al., 2005). For a given angular speed, the energy will diminish steeply with $\theta_\star \propto \tau_s$. or

$$\epsilon_{swing} \propto \frac{1}{\theta_\star^4} \ , \tag{2.4}$$

where $\theta_\star$ is the angular coordinate at the transition from the first single stance to the double stance. For geometrical reasons, just like θ_{off}, $\theta_\star$ doesn't vary much between different gaits, but it does increase slightly (Figure 4B) as one decreases $\delta_\star$. Since an increase in γ decreases $\delta_\star$, gaits with higher γ are preferred.

To investigate the range of speed allowed using the M-shaped GRF pattern, we found the limit cycles for the range of relative step lengths (λ) in our experimental data. The allowed region for M-shaped (normal human walking) (Figure 3C) shows that as λ decreases, the lowest value of γ allowed increases. The maximum and minimum Froude numbers (Fr) (Figure 3D) show that DSLIP is a good model at lower speeds but is limited at higher speeds. The range of allowed speeds is low even after considering different λ values. Compared to the previous study (Antoniak et al., 2019) which assessed the range of Fr numbers allowed using constraints on the single stance, i.e., without any requirement for limit cycles (Antoniak et al., 2019), the allowed speed is not altered at the lower end of the speed range but is altered at the higher end of the speed range. Essentially, DSLIP is an adequate model for walking at slow speeds whether one considers just the synchronization of radial

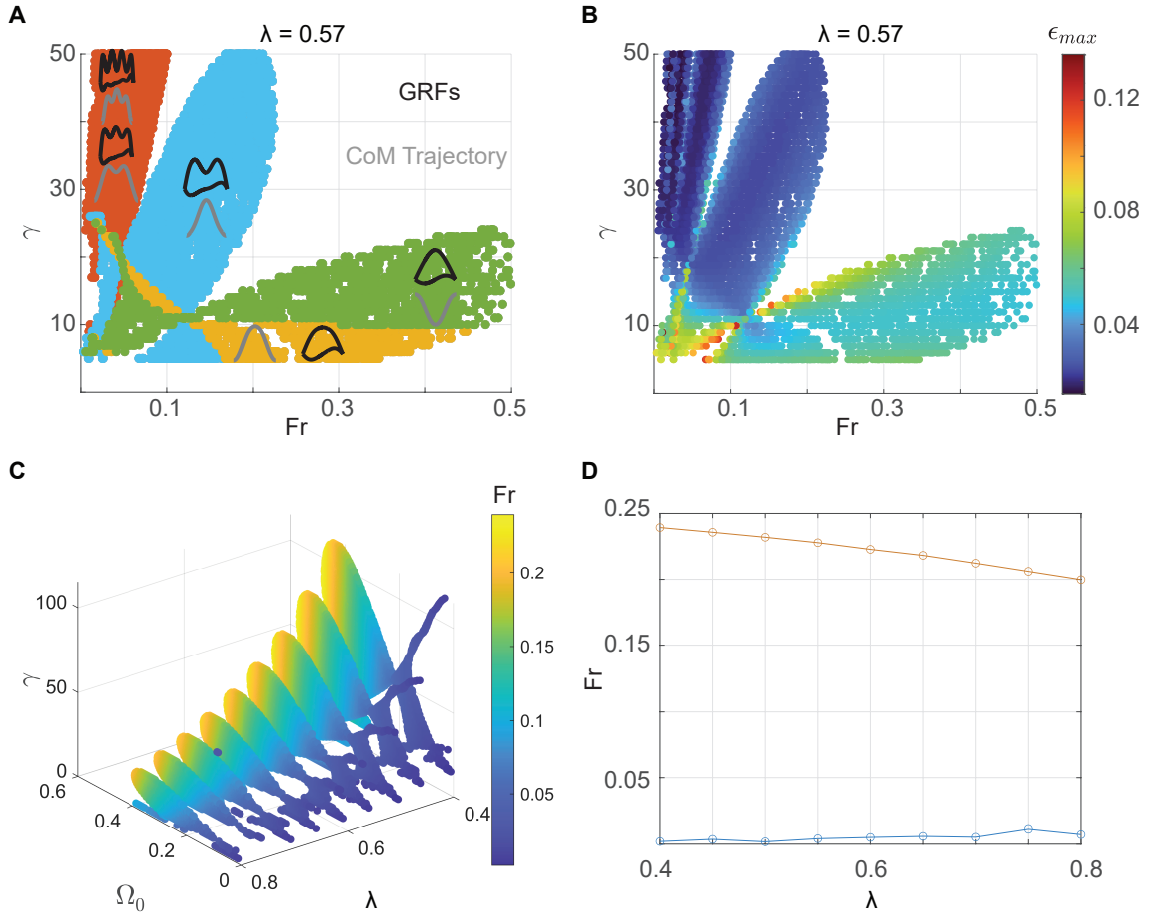

Figure 3. M-shaped walking only occurs only over a limited range of speeds over which it is energetically favored. A. Solution space for a fixed value of dimensionless step-length, selected according to the best fit to the experimental data for the preferred walking speed of our subject. Four walking modes are shown - three modes from Figure 2 and one mode with multiple oscillations. The vGRF is shown in black, and the CoM profile is in gray. **B.** The same plot as A, with colors specifying the maximum energy stored in the leg during a cycle shows the M-shaped GRF is the most energy efficient over the range of speeds for walking. **C.** The solution space for M-shaped GRFs for different step lengths. The spring stiffness changes with speed. **D**. The M-shaped walking observed in humans is limited to a Fr of 0.25 across step lengths.

and horizontal motions during the single stance or the full gait cycle. In contrast, the range of speed at the high end dramatically decreases when the double stance phase is included, a topic discussed at length in the next section.

2.2 Constraints from synchronization of radial and angular motion in single stance and velocity redirection in double stance limit DSLIP normal walking speed

Synchronization between radial and angular motion during the single stance describes the lower limits of speed possible with M-shaped GRF

DSLIP correctly predicts that M-shaped GRF walking is only possible for a limited range of speeds. To understand the mechanical constraints that limit the range of speeds for M-shaped walking, we sought an analytical approximation of the DSLIP model. The analytical approximation has two parts that correspond to single and double stance phases, respectively (see Appendix B for details). First, during the single stance phase, we assume that the angular and radial motion are decoupled. When there is no angular motion, and $\theta \approx 0$, the equation of radial motion can be written as

$$\ddot{\delta} = -\gamma\left(\delta - \frac{1}{\gamma}\right) \Rightarrow \delta = \frac{1}{\gamma} + \left(\delta_0 - \frac{1}{\gamma}\right)\cos(\omega t)\ , \text{ where } \omega \equiv \sqrt{\gamma}\ . \tag{2.5}$$

In other words, δ simply oscillates around its equilibrium value, $1/\gamma$. Further, under the approximation that angular speed is constant, we have

$$\theta = \Omega_0 t\ . \tag{2.6}$$

The oscillation phase of the radial motion can be defined as

$$\phi \equiv \omega t\ . \tag{2.7}$$

If $\phi_\star$ and $t_\star$ denote the oscillatory phase and time when the single stance transitions to the double stance, at this same time the angular motion must traverse up to the transition angle, $\theta_\star$ (Figure 4A):

$$t_\star = \frac{\phi_\star}{\omega} = \frac{\theta_\star}{\Omega_0}\ . \tag{2.8}$$

In other words, γ and Ω_0 are related as

$$\Omega_0 = \left(\frac{\theta_\star}{\phi_\star}\right)\sqrt{\gamma}\ . \tag{2.9}$$

This equation implies that as speed (Ω_0) increases, the leg must oscillate faster in the radial direction along the leg-length to keep up, leading to a larger stiffness (γ). The relationship between (Ω_0) and (γ) is more complex as $\theta_\star$ and $\phi_\star$ are not constants but rather given by (see Appendix B):

$$\sin\theta_\star = \frac{\lambda^2 + (1-\delta_\star)^2 - 1}{2(1-\delta_\star)\lambda}\ , \text{ and } \cos\phi_\star = -\left(\frac{\gamma\delta_\star - 1}{1-\gamma\delta_0}\right)\ . \tag{2.10}$$

Briefly, the $\theta_\star$ equation above results from the transition geometry (Figure 4A), and $\phi_\star$ from Eqn. (2.5). Since $\delta_\star$ is typically small and ranges between $1/\gamma < \delta_\star < 2/\gamma \ll 1$, $\theta_\star$ does not change much; there is a small increase with decreasing $\delta_\star$ (Figure 4B). Assuming $\gamma \gg 1$, we have

$$\frac{\lambda}{2}\left(1 - \frac{2}{\gamma\lambda^2}\right) \gtrsim \sin\theta_\star \gtrsim \frac{\lambda}{2}\left(1 - \frac{4}{\gamma\lambda^2}\right)\ , \tag{2.11}$$

As γ increases, $\delta_\star$ becomes smaller, and accordingly $\theta_\star$ increases towards $\sin^{-1}(\lambda/2)$.

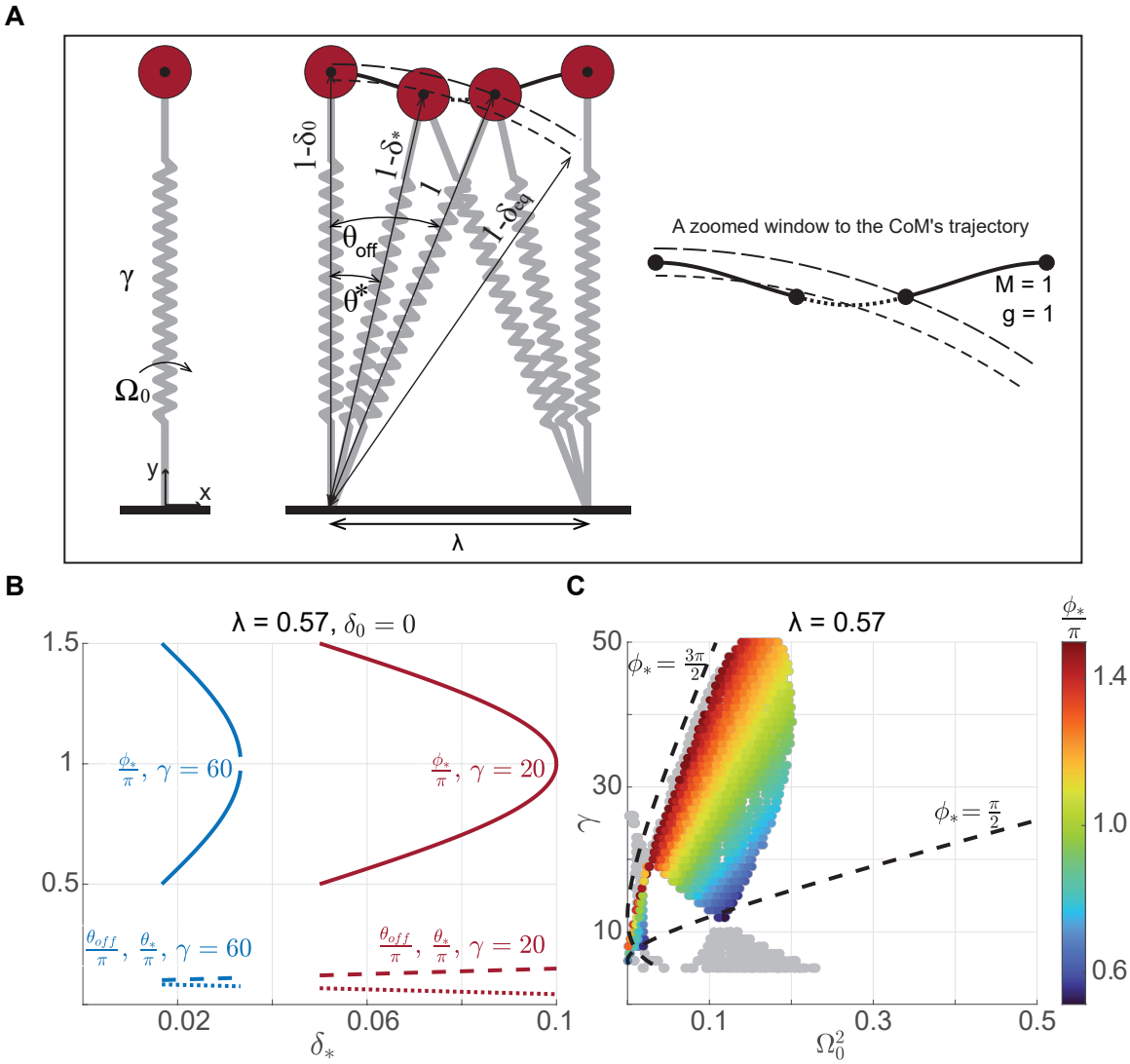

Figure 4. Synchronization between radial and angular motion divides the gaitspace into regions in which different modes are expected. A. An example simulation to illustrate synchronization between radial and angular oscillation (middle panel, zoomed version on the right). At a given step-length and leg-contraction at mid-stance, any γ and Ω_0, only solutions that have synchronized radial and angular motion can become a limit cycle. During the time it takes to travel from midstance to the transition between single and double stance phases - denoted by the starred variables, the angular coordinate must go from midstance to $\theta_\star$. The radial coordinate will go from its position between the natural length and equilibrium length at midstance to a position slightly below it. This corresponds to a change in the value of ϕ from 0 at midstance to $\frac{\pi}{2} < \phi_\star < \frac{3\pi}{2}$ at the transition. **B.** Two examples based on analytical results show that while $\phi_\star$ approximately accesses the entire range defined for normal walking, θ_{off} and $\theta_\star$ slightly increases and decreases respectively. **C.** In the figure, only solutions with $\frac{\pi}{2} < \phi_\star < \frac{3\pi}{2}$ are shown by color bar; the others are gray. Analytical constraints from synchronization are shown by the dashed line, which is close to the lower bound on speed. However, there is no limit on the upper bound. Note that at high γ, there are no limit cycle solutions close to $\phi_\star = \frac{\pi}{2}$.

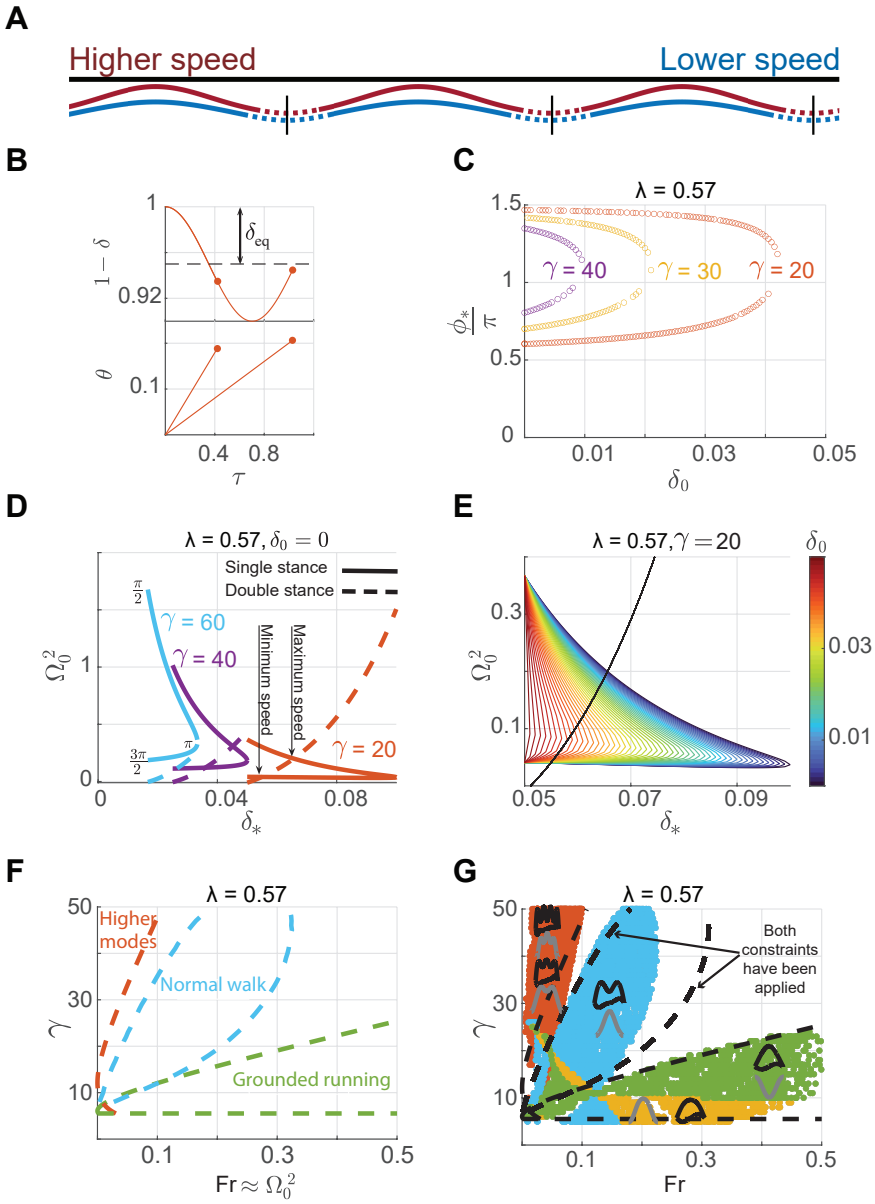

Figure 5. M-shaped walking is limited to low speeds because of a combination of synchronization and velocity redirection constraints. A. Two CoM trajectories illustrate the single stance (solid lines) and the double stance (dotted lines) phases. The double stance phase gets shorter with increasing speeds. The vertical black lines specify the mid-step. **B.** The figure shows the approximate evolution of δ and θ during the single stance phase. There are only two solutions once γ, δ_0, λ are fixed. **C.** The variation of $\phi_\star$ vs. δ_0 for a given step-length for the normal walking gait. By increasing γ, generally the speed increases, and for a given gamma, as the speed increases $\phi_\star$ and δ_0 values get closer to π and zero respectively. **D.** A graphical representation of how single (solid line) and double stance (dashed line) constraints affect the range of possible speeds. Here $\delta_0 = 0$. The highest speed possible (intersection) is much smaller than the highest speed from just single stance considerations(obtained at $\delta_\star = \frac{1}{\gamma}$). The difference becomes more with higher stiffness until at the highest stiffness (light blue, $\gamma = 60$), there is no solution (no intersection point). **E.** All solutions for a fixed step-length and stiffness. Note the double stance constraint is independent of δ_0. **F.** The region of different gait patterns that is estimated by our analytical approximation. The boundaries for normal walking become highly constrained. The other boundaries - for grounded running and higher modes - are a result of single stance constraint alone. **G.** Analytical boundaries of walking solutions from F overlayed on the numerical solution for comparison.

In contrast to the small $\theta_\star$ range, $\phi_\star$ changes considerably (Figure 4B). When $\cos\phi_\star$ is negative (we will justify this in the next subsection), $\phi_\star$ can, a priori, take any value in the range

$$\frac{\pi}{2} < \phi_\star < \frac{3\pi}{2} \tag{2.12}$$

for a single radial oscillation of the COM. Moreover, (2.10) implies that as $\delta_\star$ varies, we have two branches of $\phi_\star(\delta_\star)$: a branch along which $\delta_\star$ varies between $1/\gamma$ to $2/\gamma - \delta_0$, and $\phi_\star$ varies between $\pi/2$ to π, see Figure 4B and another where $\phi_\star$ goes from π to $3\pi/2$ as $\delta_\star$ varies between $2/\gamma - \delta_0$ to $1/\gamma$.

We can estimate the speed bounds based on the analytical equations above. It is clear from (2.9) that Ω_0 decreases if $\phi_\star$ increases and $\theta_\star$ decreases, however, the effect of $\phi_\star$ change is much larger. Thus approximately the lower-bound on speed is attained at $\delta_\star \to 1/\gamma$, and $\phi_\star \to 3\pi/2$ following the upper branch, and yielding

$$\Omega_0 \gtrsim \left(\frac{2}{3\pi}\sin^{-1}\left[\frac{\lambda}{2}\left(1-\frac{2}{\gamma\lambda^2}\right)\right]\right)\sqrt{\gamma}\ . \tag{2.13}$$

In a similar way, the upper bound is attained as $\delta_\star \to 1/\gamma$, and $\phi_\star \to \pi/2$:

$$\Omega_0 \lesssim \left(\frac{2}{\pi}\sin^{-1}\left[\frac{\lambda}{2}\left(1-\frac{2}{\gamma\lambda^2}\right)\right]\right)\sqrt{\gamma}\ . \tag{2.14}$$

The upper and lower bounds resulting from this synchronization are plotted in Figure 4C. The analytical lower bound derived above matches the simulation results well, implying that the analytical approximation captures the mechanics well. However, the analytical upper bound does not match the bounds obtained through simulation. This mismatch occurs because, except for low γ, the allowed $\phi_\star$ does not reach $\pi/2$; the allowed $\phi_\star$ deviates further from $\pi/2$ as γ increases. Single stance mechanics do not constrain the speed for normal walking; instead, as we will see next, constraints from double stance limit $\phi_\star$ This result explains why a previous study that considered only the single stance phase came to the conclusion that DSLIP can function as a model for walking even at high speeds (Antoniak et al., 2019).

Limits of DSLIP on speed result from a combination of synchronization and the requirement to redirect vertical velocity component during the double stance phase

Thus far, we have investigated how synchronization between the horizontal and vertical motions of the CoM in the single stance phase delineates the regions in the $\gamma - \Omega_0$ space where different gaits will be observed. The speed range over walking is further constrained by the need to reorient the velocity vector during double stance: The vertical CoM velocity, which is pointed downwards at the beginning of the double-support phase, must be redirected upwards by the end of the double-support phase (Geyer et al., 2006); the required redirection increases with speed. As the speed increases, this redirection becomes more difficult because the double-support phase becomes shorter, and the required change in velocity is larger (Figure 5A). We first explain this idea conceptually (Figure 5A): As speed increases, γ increases as well, and so does the equilibrium height $(1 - 1/\gamma)$. Moreover, as the radial motion of the CoM is approximately oscillating with an amplitude less than $1/\gamma$, the CoM trajectory is closer to the natural leg length at higher speeds (Figure 5A), $r \lesssim 1-2/\gamma$. Consequently, the transition geometry dictates that the transition occurs closer to the mid-step at higher speeds, when the two legs are almost of equal length. This change, in conjunction with increased horizontal speed, implies that less time is spent in the double support phase. At the same time, as the vertical component of velocity increases with the overall speed-increase, a larger change in speed is required at the double-to-single stance transition. A larger speed change in a shorter time necessitates a larger force to produce a larger acceleration. A back of the envelope calculation is instructive: The double support phase duration, $t_d \sim \delta\theta/\Omega_0$ keeps shrinking as speed increases while the required change of vertical velocity necessary during the double support phase increases, $\delta v \sim 2\Omega_0 \sin\theta_\star$.

Thus the average upward acceleration that one needs, $\sim \delta v/t_d \approx \Omega_0^2 \sin\theta_\star/\delta\theta$, increases with speed. Crucially, the increased acceleration cannot be produced because the force that can be generated during normal walking is bounded and is equal to the weight.

The above arguments do not incorporate two important effects: First, the oscillatory radial motion can flatten the trajectory, which, in turn, may reduce the required vertical speed change. Second, the bound of the maximal radially outward force comes from the approximate oscillatory dynamics, but obviously, during the double stance phase, both legs are on the ground, which can therefore provide larger upward forces. Below we provide an approximation and provide an analytic condition determining the maximum speed bound for the normal walking gait.

Limit Cycle constraint combining the single and double stance synchronization dramatically reduces the solution space

To estimate the speed bound we will first derive an approximate analytical solution for limit cycle, and then use this analytical solution to estimate the speed bound. The horizontal speed and vertical acceleration are approximately constant during the double-stance phase and equal to their value at the transition between single-stance and double-stance phase: $v_x \approx v_{x\star}$ and $a_y \approx a_{y\star}$. In particular, this implies that at the transition, the vertical acceleration must be upwards to make the velocity redirection possible, or $a_{y\star} > 0$. For an approximately simple harmonic radial oscillation, this occurs during the phase, $\frac{\pi}{2} \lesssim \phi_\star \lesssim \frac{3\pi}{2}$, thereby justifying the assumption (2.12) we made earlier. Using these approximations, and the fact that in the time the leg has to travel horizontally to the mid-step from the transition point, the upward force must be sufficient to bring the downward velocity at transition to zero at mid-step, we can derive the relationship $\Omega_0(\delta_0, \delta_\star, \gamma, \lambda)$ (see Appendix C for the derivation) as

$$\Omega_0^2 = \frac{(\gamma\delta_\star \cos\theta_\star - 1)[\lambda/2 - (1-\delta_\star)\sin\theta_\star]}{(1-\delta_\star)^2 \sin\theta_\star \cos\theta_\star} \equiv G_D(\delta_0, \delta_\star, \gamma, \lambda) \ . \tag{2.15}$$

This nonlinear function determining Ω_0 as a function of $\delta_0, \delta_\star, \gamma, \lambda$ describes the speed based on the double stance constraint. Because $\delta_\star \ll 1$ and $\theta_\star$ approximately remain a constant, the first term (the net upward force) in the numerator is the most important for determining speed, and this will be important later.

The synchronization relation obtained from the single stance phase is also a function of $\delta_0, \delta_\star, \gamma, \lambda$:

$$\Omega_0^2 = \left(\frac{\theta_\star}{\phi_\star}\right)^2 \gamma \equiv G_S(\delta_0, \delta_\star, \gamma, \lambda) \ . \tag{2.16}$$

Thus, in order to have a synchronized limit cycle, the four parameters, $\delta_0, \delta_\star, \gamma, \lambda$ must be related,

$$G_D(\delta_0, \delta_\star, \gamma, \lambda) = G_S(\delta_0, \delta_\star, \gamma, \lambda) \ , \tag{2.17}$$

leaving only three independent parameters, $\delta_0, \gamma, \lambda$. For a given δ_0 and γ, inverting the cosine function in (2.10) while obtaining $\phi_\star$ results in two branches, referred to here as $\phi_u(\delta_\star) \in (\pi, 3\pi/2)$ and $\phi_l(\delta_\star) \in (\pi/2, \pi)$ (Figure 5C). Accordingly, for a given λ, γ and δ_0, the upper branch, ϕ_u, leads to a branch with lower speeds from the single stance synchronization condition (2.16),

$$\Omega_0^2 = \left[\frac{\theta_\star(\delta_\star)}{\phi_u(\delta_\star)}\right]^2 \gamma \equiv G_l(\delta_0, \delta_\star, \gamma, \lambda) \ , \tag{2.18}$$

while the lower branch leads to a branch with higher speeds,

$$\Omega_0^2 = \left[\frac{\theta_\star(\delta_\star)}{\phi_l(\delta_\star)}\right]^2 \gamma \equiv G_u(\delta_0, \delta_\star, \gamma, \lambda) \ , \tag{2.19}$$

So, if the three parameters, $\delta_0, \gamma, \lambda$ are fixed, there are only two possible values of Ω_0 resulting from two values of $\phi_\star$ and $\delta_\star$ corresponding to two branches of solution (Figure 5B); from a different

perspective, relating single and double-stance dramatically shrinks the solution space from the entire range between $\pi/2$ to $3\pi/2$ for allowed $\phi_\star$ to just two values of $\phi_\star$ (Figure 5C).

Satisfying both single stance and double stance constraints simultaneously is difficult at high speeds and curtails speeds at which walking is possible

Normal walking must satisfy both the single stance and double stance requirement (2.17). The maximum speed occurs at different $\delta_\star$ and $\phi_\star$ values for the single and double stance: Synchronization during single stance (2.16) suggests that a speed maximum is reached as $\delta_\star \to 1/\gamma$ and $\phi_\star \to \pi/2$ (Figure 5D). However, synchronization during double-stance does not allow $\delta_\star \to 1/\gamma$ and $\phi_\star \to \pi/2$: As $\delta_\star \to 1/\gamma$ - the upward force (the first term within the parenthesis in the numerator of (2.15)) becomes negative and is disallowed (see Figure 4C). Thus, it is not possible for $\phi_\star$ to attain $\pi/2$ (Figure 5C). This inability of $\phi_\star$ to reach $\pi/2$ is also reflected in the simulation results in Figure 4C and becomes worse as γ increases (Figure 4C and 5C). The maximum upward force in the double stance phase occurs at the largest compression possible, $\delta_\star \approx 2/\gamma$ when $\phi_\star \approx \pi$. In calculating the force $\delta_\star$ is multiplied by $\gamma \gg 1$, and thus, the effect of $\delta_\star$ in G_D is dominated by the force term. The maximum speed possible is a compromise between the considerations from single and double stance and the largest speed occurs at a value of $\delta_\star$ between $\pi/2$ (where the maximum speed from single stance condition occurs) and π (where the maximum speed from double stance condition occurs).

By inspection of (2.10) it is also clear that for a given $\delta_\star$, $\phi_\star$ is smallest if $\delta_0 = 0$. Thus, the maximum speed is approximately attained at a $\delta_\star$ that satisfies both (2.16) and (2.15) for $\delta_0 = 0$. Or,

$$\left(\frac{\theta_\star}{\phi_\star}\right)^2 \gamma = \frac{(\gamma\delta_\star \cos\theta_\star - 1)[\lambda/2 - (1-\delta_\star)\sin\theta_\star]}{(1-\delta_\star)^2 \sin\theta_\star \cos\theta_\star} \ , \tag{2.20}$$

where $\cos\phi_\star = -(\gamma\delta_\star - 1)$, and $\theta_\star$ is given by (2.10). (2.20) can be solved to obtain $\delta_\star$ as a function of λ and γ. Graphically, the solution is given as the intersection between curves depicting equations (2.15) and (2.19) or (2.18) (Figure 5D). The constraining function, G_D, from the double-support does not depend on $\phi_\star$, and therefore has no branches. It is a monotonically increasing function of $\delta_\star$ that can intersect both the lower and the higher branches, $G_l(\delta_\star)$ and $G_u(\delta_\star)$, leading to two possible solutions. The maximum speed is given by the intersection of these two constraints that occur between $\phi_\star$ of $\pi/2$ and π, and is, therefore, lower than the speed possible if we only consider single-stance synchronization. This decrease is exacerbated as γ increases (Figure 5D). For a given λ and large enough γ's, there are no solutions at all, consistent with our numerical findings (Figure 5D, $\gamma = 60$). The lower bound is also attained when $\delta_0 \to 0$ as that decreases $\cos\phi_\star$ so that $\phi_\star$ can get close to $3\pi/2$ (Figure 5D). The lower bound is reached when $\delta_\star$ is close to $1/\gamma$, but as argued before, the upper bound $\delta_\star$ ends up at a compromise value between $1/\gamma$ and $2/\gamma$. The effect of the double-stance constraint on the lower speed bound is much less (Figure 5D).

Essentially the same analysis can be performed for non-zero δ_0 with two limit cycles possible for a given value of δ_0. More generally, the double-valued nature of $\phi_\star(\delta_\star)$ leads to a double-valued $\delta_\star(\delta_0)$ function (Figure 5E) resulting in a family of curves - one for each δ_0.

The overall results are summarized in Figures 5F and 5G. The single stance constraint alone divides the gait space into contiguous regions with different oscillatory gaits (Figure 4C). Addition of the double stance constraint limits the region allowed (Figure 5F). The results from the analytical approximation of DSLIP and the actual simulations are overlayed in (Figure 5G). The range of speeds predicted from the analytical consideration (see Appendix C for more details) matches the simulation results closely. The correspondence is particularly close for low speeds. The small discrepancy at the higher speed is likely a result of oversimplication of the dynamics of the double stance phase. However, the critical result is that it is the differing constraints from synchronization in the single and double stance phases that limits the range of speed over which M-shaped walking is possible.

Lowerbound on γ from requirement of a double stance phase

There are two other features of the gaitspace. First, requiring a finite single stance phase places a floor on γ. To change the vertical component of the velocity during the double stance phase at the transition

$$\delta_\star \gtrsim \frac{1}{\gamma} \tag{2.21}$$

We can now use the transition geometry to find a lower bound on γ. As $\delta_\star$ increases the transition occurs at smaller $\theta_\star$ angles (2.10), also see Figure 4A. Thus if $\delta_\star$ is pushed to a very large value by decreasing γ, $\theta_\star$ will become zero, and there won't be any single stance phase at all. By setting $\theta_\star = 0$ depicting the extreme configuration when the transition to double stance occurs at the mid-stance, we get

$$\delta_{\star,\max} = 1 - \sqrt{1-\lambda^2} \gtrsim \frac{1}{\gamma} \Rightarrow \gamma > \gamma_{\min} \equiv \frac{1}{1-\sqrt{1-\lambda^2}} \approx \frac{2}{\lambda^2} \ . \tag{2.22}$$

The analysis above extends to limit cycles with multiple oscillations
The general form of solutions of (B.4) that have a leg-length minimum (or vGRF maximum) at mid-stance can be written as

$$\phi_\star = 2\pi n \pm \arccos\left(\frac{1-\gamma\delta_\star}{1-\gamma\delta_0}\right), n \in \{0, 1, \dots\} \ , \tag{2.23}$$

where we have assumed, $\gamma\delta_\star > 1$, $\gamma\delta_0 > 1$ and $\arccos(\phi)$ is defined as $\cos^{-1}\phi$ with ϕ restricted to the first quadrant, $0 < \phi < \frac{\pi}{2}$. The lowest $n = 0$ mode leads to $0 < \phi_\star < \frac{\pi}{2}$ and corresponds to the inverted gaits [1], the most commonly observed gait among these grounded-running *like* oscillatory modes. In contrast, the normal walking gait, which exhibits a leg-length maximum (or vGRF minimum) at mid-stance is the lowest oscillatory mode (n=1) among the normal-walking *like* oscillatory gaits:

$$\phi_\star = \pi(2n-1) \pm \arccos\left(\frac{\gamma\delta_\star - 1}{1-\gamma\delta_0}\right), n \in \{1, 2, \dots\} \ , \tag{2.24}$$

where now we have $\gamma\delta_\star > 1$, but $\gamma\delta_0 < 1$. The normal walking gait can thus represent solutions with $\phi_\star$ either in the second ($\frac{\pi}{2} < \phi_\star < \pi$) or the third ($\pi < \phi_\star < \frac{3\pi}{2}$) quarter of the unit circle.

The multiple branches of $\phi_\star(\delta_\star)$ lead to multiple branches of G_S as a function of $\delta_\star$, and eventually many intersections of G_S with G_D. Thus we can have many limit cycles with the same speed and δ_0 that, nevertheless, belong to different oscillatory gaits. Since the higher oscillatory modes correspond to lower G_S curves, the allowed speed range keeps decreasing as the number of oscillations increases.

There is one gait, the grounded running gait, for which the above approximate strategy fails (and is also unnecessary), as discussed in Appendix D. Essentially, in the grounded running gait, there is no longer any need to redirect the velocity in the double stance phase, and hence our analytical calculations are not valid.

2.3 DSLIP is an adequate model for human walking only for a narrow range of speeds

The analysis presented in this study thus far show that approximating walking dynamics using a spring-mass system explains features of walking, such as the use of M-shaped GRFs and the range of speeds over which humans walk. To further evaluate whether the interactions between the walker and the substrate can be quantitatively described with a spring-mass model, we next evaluated how close DSLIP came to describing the kinematics and GRFs during walking. To this end, we fit DSLIP to human walking data. Using an instrumented treadmill, we collected data for four walking

[1] Since $\phi_\star$ can only be positive, the $\phi_\star \in (-\pi/2, 0)$ is unphysical and absent from the $n = 0$ grounded running gait.

speeds - 2.0 mph, 2.5 mph, 3.0 mph, and 3.5 mph (see Supplementary Materials 4.2). Following previous work (Antoniak et al., 2019), we fit both the GRF and CoM kinematics in real-world or dimensional units and individual steps rather than the average data. Briefly, fitting just the GRF in normalized time units provides fallacious results as the R_{nat} determines the natural time scale of a pendulum. Thus varying R_{nat} tunes the natural time scale allowing fits to trajectories for a wide range of speeds. However, this is not biologically feasible as the leg length can only vary within a small range, and within the context of SLIP, R_{nat} is considered to be a fixed parameter. At the same time, choosing the height of the hip marker as the CoM is an overly stringent constraint; the marker for hip height is a good approximation for the movement of the CoM in time but not the exact CoM location. Therefore, we began by determining the optimal R_{nat} for - 2.5 mph - which was the preferred walking speed for the subject (Figure 6A).

To this end, we first fit a non-periodic trajectory, i.e., the fits were not constrained to be limit cycles, to each walking step separately, to allow more flexibility and independent assessment of the best fit over 40 steps, thereby increasing statistical power (see Supplementary Materials 4.3.1). In obtaining R_{nat}, we used four values of R_{nat}, these values were selected through trial and error. The vertical GRF was well fit at all selected values of R_{nat}, as was the height of the CoM. The highest value of R_{nat} , 128 cm, was the best fit to the horizontal GRF (Figure 6A and B), and yielded the lowest overall error, and was selected as R_{nat} of 128 cm for limit cycle fits.

After fixing R_{nat}, there remained only three free parameters that determine a limit cycle; two of them - the average step length and speed were fixed by constraining them to match the experimentally observed step length and step time. The remaining parameter is selected as the average minimum vGRF over the single stance phase, which can be directly calculated from the data as well. This parameter captures an essential feature of the vertical ground reaction forces that characterizes its "M"-shape profile and therefore seemed important to us. For more details related to optimization methods, please refer to Supplementary Materials 4.3.2.

One example of the limit cycle fit is shown in Figure 6C. A single limit cycle closely describes the entire sequence of steps rather than the average step as is typically done; as a consequence, the limit cycle fits some steps better than others. As an example, the fourth step, which is slower than the optimized limit cycle, does not fit well; but this delay is corrected by faster steps later in the sequence (Figure 6C). Overall, a single limit cycle optimized to fit the entire sequence of steps fits the data well and implies that DSLIP is an excellent model for walking at the preferred speed.

Typical single step fits, one for each of the four speeds, are shown in Figure 7A. Walking at 2.5 mph is best modeled by DSLIP; at this speed, the optimized limit cycle tracks important dynamical features such as the step length, speed, vGRF, and the single stance time (Figure S1D). The model still produces reasonable fits at both 2.0 mph and 3.0 mph, but the fits deteriorate at these speeds. At 2.0 mph, the best-fit model has a longer single stance time; the fitted vGRF oscillates somewhat more than the empirical data. The nature of the deviation is different at 3.0 mph where the model has a lower minimum in vGRF compared to the subject, and much larger oscillations of the vertical motion of the CoM. The model completely fails at 3.5 mph as the minima in the vGRF is close to zero. The average of total errors from GRFs and CoM kinematics along with parameters of optimized limit cycles, are shown in Figure 7B. The total error validates our qualitative observations above. The median error for fits at 2.0, 2.5, and 3.0 mph are at or below ten percent but are much larger for fits at 3.5 mph.

Surprisingly, the best-fit spring constant is higher for 2.0 mph (Figure 8A); this finding provides one important clue regarding why DSLIP works as a great model for walking at 2.5 mph and not other speeds. The higher spring constant is unexpected because most previous work has shown that the spring constant decreases as the speed decreases (Farley and Gonzalez, 1996; Kim and Park, 2011). Indeed, the spring constant for the single stance phase, as directly inferred from force-length curve, decreases with speed (Figure S2). At the step length used by our subject to walk at 2.0 mph, there are no limit cycle solutions for this spring constant (Figure 8B) and therefore the spring

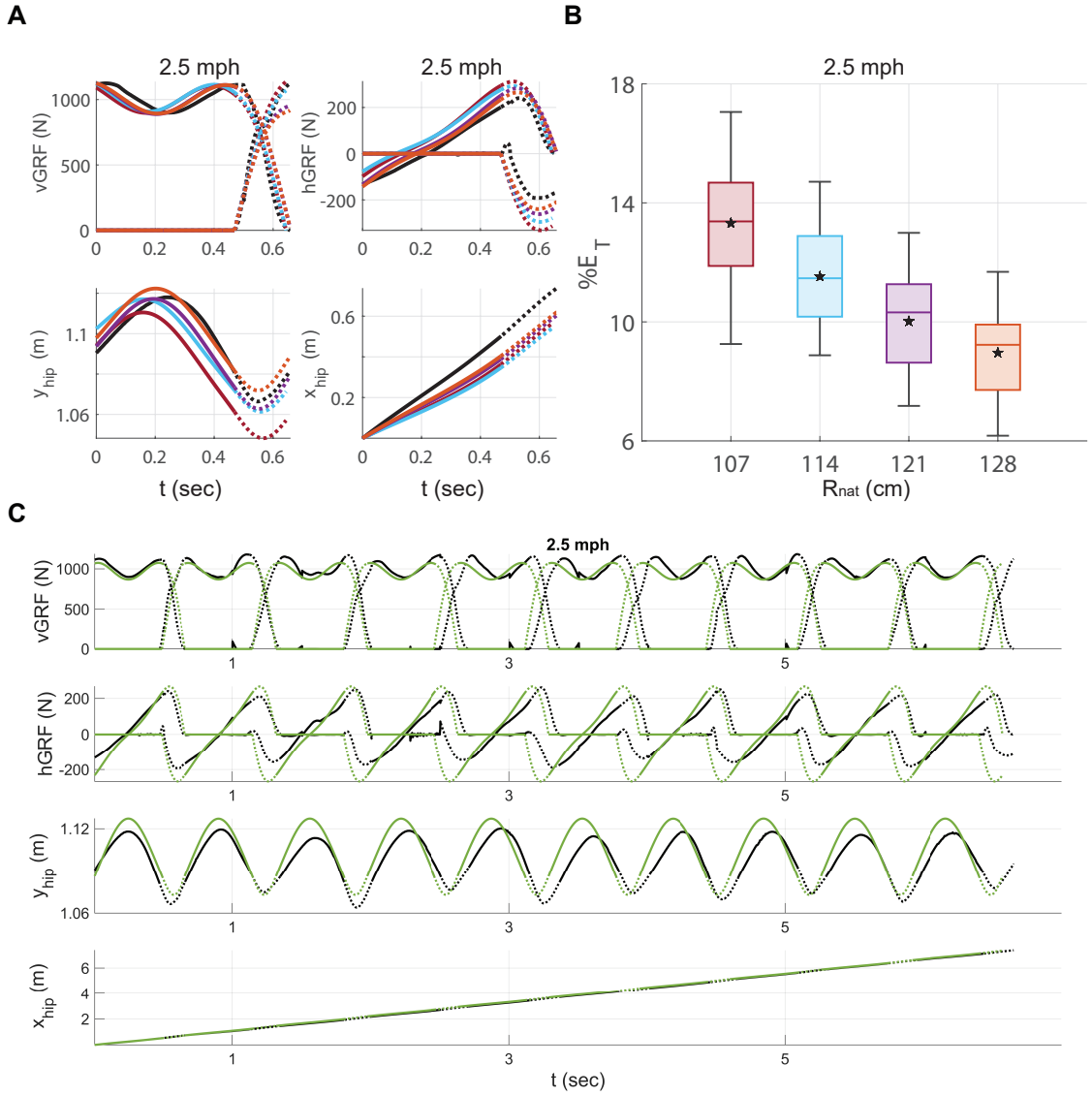

Figure 6. DSLIP is an excellent model for human walking over a narrow range of speeds. A. Since the hip marker may not be exactly at the CoM, we fit the experimental data (black lines) to a range of heights both smaller and larger than the hip height (colored lines) (see Supplementary Materials 4.3.1). Solid lines and dotted lines represent single and double stance phases respectively. **B.** The total error for each leg length shows that 128 cm has the lowest error. The error is the sum of errors related to the vGRF, hGRF, height, and horizontal displacement of the CoM. **C.** The optimized limit cycle based on $R_{nat} = 128cm$ (green lines) fits well into 10 walking steps. The total error in time is negligible.

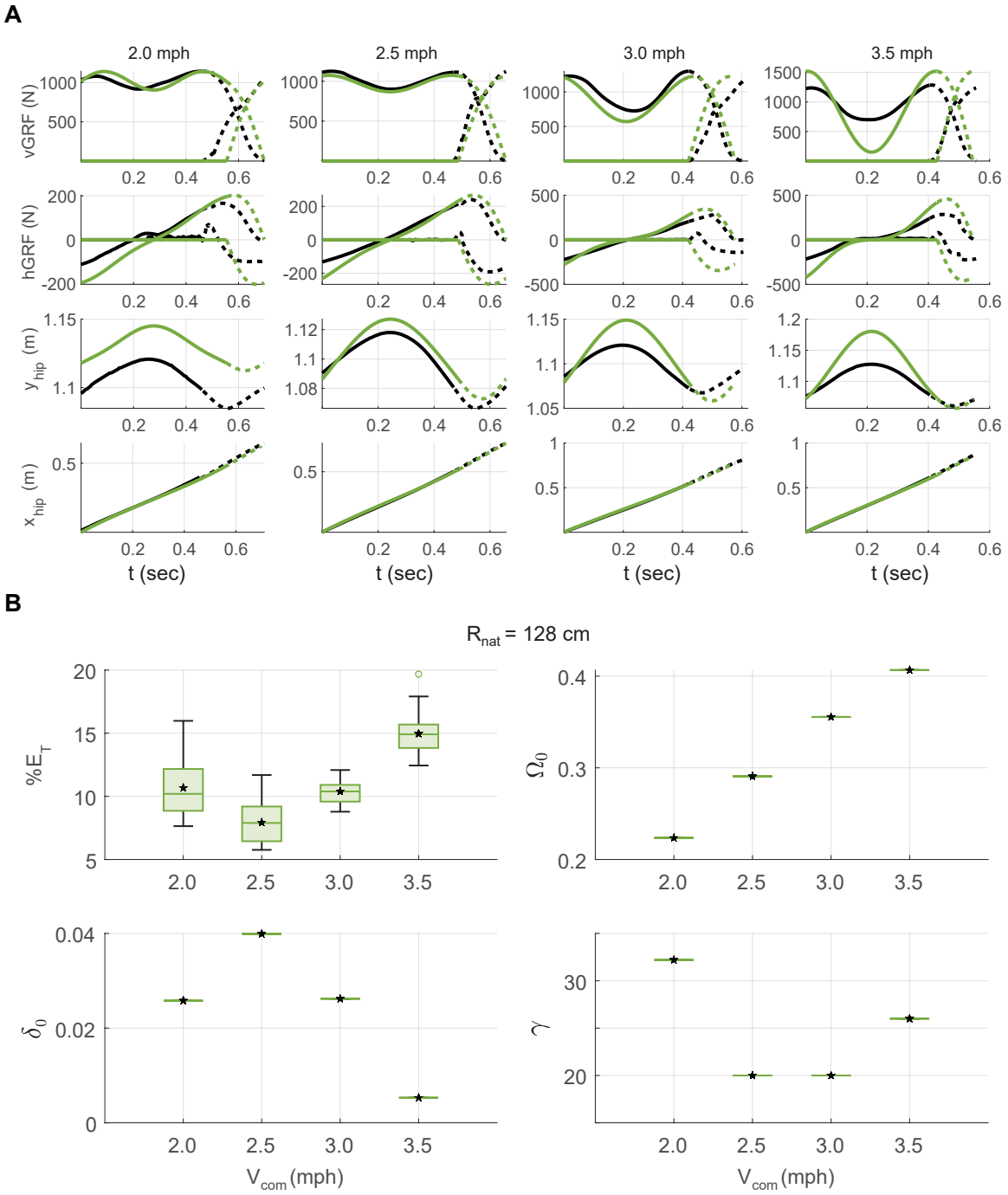

Figure 7. DSLIP fits for both lower and higher than the preferred speed are worse but for distinct reasons. A. Example fits (green lines) and data (black lines). Solid lines and dotted lines represent single and double stance phases respectively. The model and subject have the same step length and speed in all fits. We optimized limit cycles based on the values of vGRF at the mid-stance, which can be considered the only free parameter left. The best fit belongs to the preferred speed (2.5 mph), and the highest speed (3.5 mph) has the worst prediction. **B.** The total errors including GRFs and CoM kinematics along with the parameters of the optimized limit cycles for different walking speeds.

constant for the best-fit limit cycle is artificially higher. Previous work (Biswas et al., 2018) suggested that at low speeds it becomes increasingly important to model tangential forces. Their introduction may allow one to walk with lower values of γ in this low velocity regime and provide a more accurate description of the dynamics. The force-length relationship (Figure S2) also shows that at 2.5 mph, the spring constant during single and double stance phases are similar. This similarity can explain why a DSLIP model which uses a single spring constant is a quantitative model for human walking at that speed. At higher speeds, the spring constants that describe single-stance and double-stance phases become very different, and this difference makes it difficult for the DSLIP model to describe the data. The fits at 3.0 mph, has a stiffness that is approximately the average of the values in the single and double stance phase. As a result the model fit has a smaller γ than suggested from the force-length measurements in the single stance phase. With this smaller stiffness generation of the observed fluctuations in vGRF required a much larger change in the CoM height in the fits as compared to what is observed. In sum, DSLIP seem to function as a quantitative model around the preferred walking speed. At lower speeds, the range of spring constant that can lead to limit cycles shrinks. At higher speeds, the spring constants that describe single and double stance phases are different, making it difficult for DSLIP to model.

3 Discussion

3.1 A compliant leg is necessary for modeling many features of locomotion

A model with non-compliant legs – IP – continues to persist as a model for walking. The IP model has been successful in explaining the energetics of walking (Donelan et al., 2002; Kuo, 2002; Kuo et al., 2005). The inability of IP model to describe forces is considered a surmountable limitation. Proponents of IP have argued that this limitation of IP arises from the impulsive nature of work in the IP model, and that if this constraint is relaxed, variations of IP model can recover the M-shaped GRF observed during walking. However, we show here that a compliant leg provides two important advantages. First, by providing a means to relate leg stiffness that controls the amplitude and period of the vertical oscillation to the angular speed of stance progression, they provide an analytical framework rooted in mechanics for analyzing which gaits will be observed. Second, leg compliance also provides a mechanism for understanding limitations faced in the redirection of velocity vector. It is clear from the analysis performed in this study that the challenges with redirecting the velocity vector limits the range of speeds over which humans can walk. We also show here that the energetics of a compliant leg is necessary for understanding why a particular gait, defined by GRF and kinematics, is observed in a given step during walking as well. Its relative simplicity and flexibility make it an ideal jumping board for more complex models of locomotion.

3.2 M-shaped GRFs are prevalent because they are energetically efficient

An unexplained characteristic of human walking is that humans walk with a M-shaped GRF profile. The M-shaped GRF is observed in other walkers including both bipeds and quadrupeds (Andrada et al., 2013a, 2014; Basu et al., 2019). At the speeds at which humans walk, other modes of walking, such as grounded running, are possible. However, the M-shaped profile is energetically favored. We have shown that the normal walking gait has a stiffer leg as compared to grounded running, which is preferred because a stiff leg results in smaller vertical oscillations and therefore ultimately less work[2]. This same logic would posit that even higher modes of oscillation with even stiffer legs would be more energy efficient than the normal gait. While this is true and we do see that at very slow speeds multi-oscillatory gaits may be preferred (Figure S3), these gaits are not available at typical walking

[2]While work is proportional to the force, it is proportional to the square of the contraction.

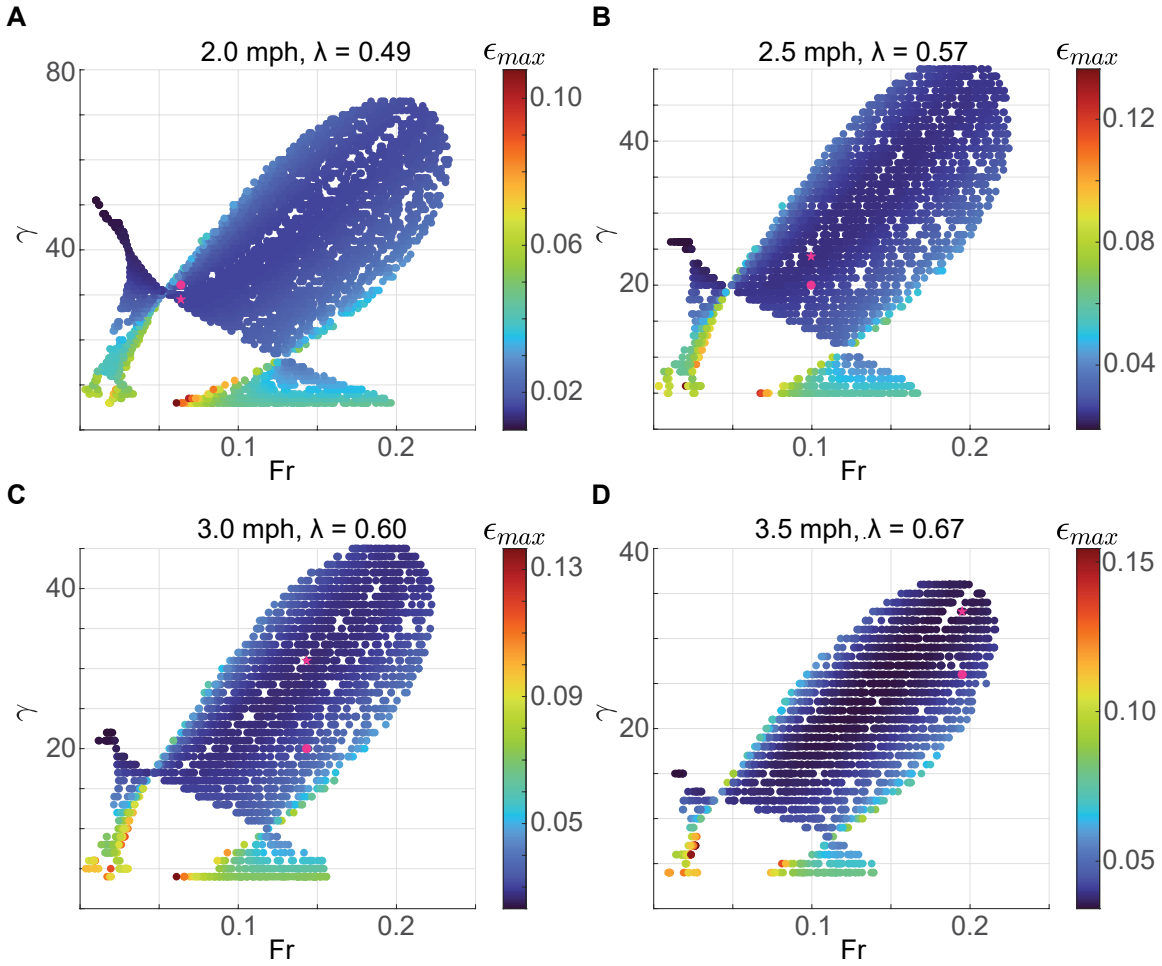

Figure 8. The range of spring constant where a limit cycle is possible likely makes it difficult to obtain good fits for human walking. A, **B**, **C**, and **D** belong to the 2.0, 2.5, 3.0, and 3.5 mph walking speeds of the subject, respectively. The pink circles show the optimized limit cycles based on our method, and the pink stars show the limit cycles with the minimum energy at the same speed. Black crosses demonstrate optimization outputs for non-periodic trajectories. At both 2 mph and 3.5 mph, the optimization solutions are close to the solution boundary.

speeds because of a gait-specific speed bound that results from the velocity redirection requirement as we now discuss.

3.3 Gait transition occurs because velocity redirection is difficult

An important issue that has received much attention is gait transitions: at what speeds do they happen and why? One approach to this problem is using the IP model. Walking using an IP model is not possible at high speeds because at high speeds – above Fr of 1 - the centripetal force needed exceeds the gravitational forces. This logic was later modified to take into account the fact that the vertical component of the gravitational force would be lowest near the end of the step. While taking this into account it is possible to produce a walking step with Fr ~ 0.5, such steps involves large changes in horizontal speed, completely uncharacteristic of biological walking trajectories (Usherwood, 2005). Analysis in this study using the DSLIP model comes to a very different conclusion. First, even if we take a nuanced approach to walking and impose the condition that walking must have a vGRF minimum at mid-stance, centripetal force does not pose a stringent constraint (see Figure 4C). Moreover, DSLIP makes it possible to walk with gaits that are not possible using the IP model such as the grounded running gait. In sum, adding compliance to the leg removes the appearance of unphysical negative tension force as a reason for gait transition. Our analysis of the DSLIP model suggests a completely different reason for gait transition. Walking with a M-shaped GRF necessitates velocity redirection. Velocity redirection becomes more difficult as speed increases. This inability to perform velocity redirection limits speeds at which walking with M-shaped GRF is possible. There are two options when transitioning from M-shaped walking: Transition can be to other modes without an aerial phase such as grounded running and inverted walking. Alternatively, the transition from M-shaped walking can be to locomotion with an aerial phase. Thus, analysis using DSLIP model suggests two different answers to gait transitions: Transitions out of M-shaped GRFs occur at low speeds, transitions from locomotion without an aerial phase to one with an aerial phase can occur at any speed. As an example, both grounded running and aerial running can occur over a large range of speeds.

At what speed aerial running occurs depends on the individual and species. In humans, transitions can occur from M-shaped walking to aerial running as is suggested by some. Under certain conditions, there is a small range of speed over which humans walk with a grounded running gait (Shorten and Pisciotta, 2017; Bonnaerens et al., 2019). In many birds, grounded running is preferred over a large range of speeds often exceeding a Fr of 1 (Andrada et al., 2020). Many non-human primates also prefer grounded running (Blickhan et al., 2018). Fast-running insects and spiders prefer grounded running (Reinhardt and Blickhan, 2014). To address which gait is preferred energy estimates for aerial and grounded running at a given speed must be made, which is beyond the scope of this paper.

3.4 Limitations of DSLIP and how they might be overcome

DSLIP is a great conceptual model, but with its simplicity comes some limitations. Although DSLIP does predict that the walk-to-run transition comes from the inability to change the velocity from one step to the next, the speed at which this transition occurs is lower than what is typically observed. DSLIP cannot support walking above a Fr number of 0.25 whereas humans can walk with M-shaped GRF till a Fr number of 0.45 (Kram et al., 1997). There are many mechanisms that might contribute to humans walking at higher Fr numbers. One mechanism is that human legs are not massless, and recoil from the leg swinging forward contributes to velocity redirection (Adamczyk and Kuo, 2009). Another mechanism is that the center of pressure moves forward during stance; this forward movement might increase the range of speeds.

All of these processes can be modeled as additions to the SLIP model and aspects of these pro-

cesses have been explored by others (Whittington and Thelen, 2009; Lim and Park, 2019; Mauersberger et al., 2022). Adding features to the model will increase model complexity. If complexity is desired, DSLIP is likely the best base model. However, there are additions that might be highly beneficial without increasing model complexity unduly. One addition is to use a variable spring stiffness. Plotting the relation between change in leg length and force, the slope of which is a surrogate for the spring constant, suggests that at high walking speeds both the spring constant and the natural leg length during the single and double stance phases are different (Figure S2). This difference suggests that changing the stiffness and natural length of the spring during the double stance phase may be a mechanism for increasing the speed over which M-shaped GRF walking gaits are possible. Note, that the M-shape is essentially guaranteed by having a a minimum at mid-stance during which the dynamics would be identical to DSLIP, and then having a single oscillatory cycle between the mid-stance and take-off.

Another mechanism is adding an angular spring. As has been noted previously, net forces during walking do not point along the leg but are more vertical (Maus et al., 2010; Müller et al., 2017; Antoniak et al., 2019). This limitation can be addressed by adding an angular spring as we have proposed earlier (Biswas et al., 2018; Antoniak et al., 2019). An angular spring produces restorative forces such that there is no angular force at mid-stance. The angular forces increase as the leg moves away from mid-stance. As investigated in (Biswas et al., 2018), such angular forces can provide a much wider range of realistic gaits at low speeds.

4 Material and Methods

In this section, we briefly describe the model, the essential details related to the empirical data, and the numerical techniques to find walking solutions and optimized trajectories.

4.1 Walking dynamics of DSLIP

In this paper, we reconsider and reevaluate the simplest human walking model introduced by Geyer et al. (Geyer et al., 2006). The model is capable of presenting periodic walking gaits with the fewest set of parameters while keeping important features of human walking such as M-shaped vGRF and CoM trajectory. This model is a basic model for running as well and is able to exhibit other common bipedal gaits with a few modifications (Gan et al., 2018). It is a two degrees of freedom (DoF) model that describes the planar motion of a point mass merely under gravity and spring forces.

4.1.1 The equations of motion

The model in its full dimension and dimensionless form is shown in Figure 1A and Figure 4A respectively. Figure 1A is a schematic but Figure 4A is drawn based on simulation. The model consists of two mass-less springy legs hinged with a large mass, M, at the hip (CoM). The model does not include any swing phase dynamics, so the single stance phase is described by just a single spring with the mass at the top. The natural leg length of the springs is shown by R_{nat}. The leg stiffness, K_s, and the step length, L, are made dimensionless according to the following equations:

$$\gamma = \frac{K_s R_{nat}}{Mg}$$
$$\lambda = \frac{L}{R_{nat}} \tag{4.25}$$

where g is the gravitational acceleration. To show the dimensionless parameters in the figure, the values of R_{nat}, M, and g are supposed to be 1. The motion starts from the mid-stance, i.e when

the stance leg stands upright. The dynamics during the single stance phase evolve according to the following equations represented in the Cartesian form:

$$\ddot{x} = \frac{\gamma x(1-\sqrt{x^2+y^2})}{\sqrt{x^2+y^2}}$$
$$\ddot{y} = \frac{\gamma y(1-\sqrt{x^2+y^2})}{\sqrt{x^2+y^2}} - 1 \tag{4.26}$$

where x and y show the dimensionless form of horizontal and vertical displacement of the CoM respectively:

$$x = \frac{X_{com}}{R_{nat}}$$
$$y = \frac{Y_{com}}{R_{nat}} \tag{4.27}$$

Also, we made the time dimensionless by using the following relationship:

$$t^{'} = t\sqrt{\frac{g}{R_{nat}}} \tag{4.28}$$

Then, the initial conditions are defined by the position and velocity of the CoM at the mid-stance:

$$x_0 = 0$$
$$\dot{x}_0 = (1-\delta_0)\Omega_0$$
$$y_0 = 1-\delta_0$$
$$\dot{y}_0 = -\dot{\delta}_0 \tag{4.29}$$

where δ_0 and Ω_0 are the initial dimensionless spring contraction and angular velocity at the mid-stance, respectively. With appropriate parameters and acceptable initial conditions, the walker is able to continue the single stance phase until the leading leg successfully touches the ground. It is supposed that the touch-down event is recognized by a predefined step length, which can be respected as a very simplified foot placement strategy. At this moment, the following algebraic equation is satisfied by the CoM position:

$$(\lambda - x)^2 + y^2 = 1 \tag{4.30}$$

In contrast to rigid inverted pendulum walking models, this impact is conservative, so the CoM begins the double support phase without any energy loss. However, since both the velocity and acceleration of the swing foot get zero, the governing equations of motion switch to the new ones:

$$\ddot{x} = \frac{\gamma x(1-\sqrt{x^2+y^2})}{\sqrt{x^2+y^2}} - \frac{\gamma(\lambda-x)(1-\sqrt{(\lambda-x)^2+y^2})}{\sqrt{(\lambda-x)^2+y^2}}$$
$$\ddot{y} = \frac{\gamma y(1-\sqrt{x^2+y^2})}{\sqrt{x^2+y^2}} + \frac{\gamma y(1-\sqrt{(\lambda-x)^2+y^2})}{\sqrt{(\lambda-x)^2+y^2}} - 1 \tag{4.31}$$

When the contact force at the trailing leg gets zero, the leg reaches its natural length and leaves the ground. This moment is called toe-off and is detected by a simple geometric formula:

$$x^2 + y^2 = 1 \tag{4.32}$$

Then the single stance phase restarts by resetting the coordinate to the new contact point. In this regard, despite the CoM's velocity continuity, it experiences a discontinuity in its position according to the following equation:

$$x^+ = x^- - \lambda \tag{4.33}$$

where x^+ and x^- are the x-component of CoM just after toe-off and before it respectively. The gait cycle ends when the stance leg re-stands vertically ($x = 0$). Now, we can summarize all equations in a single Poincaré return map which maps the states from i^{th} mid-stance to $(i+1)^{th}$ mid-stance:

$$q_{i+1} = S(q_i) \tag{4.34}$$

where:

$$q = \{0, \dot{x}_0, y_0, \dot{y}_0\} \tag{4.35}$$

At a fixed point which represents a limit cycle we have:

$$q^* = S(q^*) \tag{4.36}$$

where:

$$q^* = \{0, \dot{x}^*, y^*, \dot{y}^*\} \tag{4.37}$$

4.1.2 Parameters and Conditions for symmetric human-like limit cycle walking

Steady-state human walking is so close to a symmetric and periodic locomotion. Employment of this fact helps to reduce the complexity and the number of independent parameters. So it is worthwhile to focus on symmetric limit cycle solutions. To this end, the first derivative of vGRF must be zero at mid-stance. So we have:

$$\dot{F}_y = 0 \Longrightarrow \dot{y} = 0 \quad at \quad x = 0 \tag{4.38}$$

As a result, the general form of initial conditions for equations (4.26) will be:

$$[x_0, \dot{x}_0, y_0, \dot{y}_0] = [0, (1-\delta_0)\Omega_0, 1-\delta_0, 0] \tag{4.39}$$

Now, since we just look for limit cycles, there must be a relation between δ_0 and Ω_0 to synchronize the radial displacement of the spring with its rotational movement; so the real number of independent parameters for dimensionless symmetric limit cycle walking will be restricted to three; which can be any three of the following four parameters:

$$P = \{\lambda, \gamma, \Omega_0, \delta_0\} \tag{4.40}$$

Furthermore, to have human-like solutions, i.e. limit cycles with M-shaped vGRF and maximum height profile at the mid-stance, another constraint must be applied to parameters to restrict the solution space. This means that $\ddot{F}_y \geq 0$ and $\ddot{y} \leq 0$ leading to the following inequality:

$$\gamma\delta_0 \leq (1 - \Omega_0^2) \tag{4.41}$$

4.1.3 Finding Limit cycles

In general, finding limit cycles is not easy; especially for unstable trajectories. If the DoF is low, and if we have a good estimation of initial conditions, it will be easier to find them. Based on trial and error or using analytical approximations, we can find such an estimation around the desired fixed point which represents a limit cycle. At a fixed point we have:

$$q^* = S(q^*) \tag{4.42}$$

where:

$$q^* = \{0, \dot{x}^*, y^*, 0\} \tag{4.43}$$

This fixed point represents the initial condition that leads to a symmetric periodic gait. To find the fixed point and analyze its stability, we engage a method described in (Wisse et al., 2004). To explain the method in detail, a small perturbation is added to the fixed point at step i as follows:

$$q^* + \Delta q_{i+1} = S(q^* + \Delta q_i) \tag{4.44}$$

Now, by using the Taylor expansion of Poincaré map around the fixed point we have:

$$q^* + \Delta q_{i+1} = S(q^*) + J\Delta q_i \tag{4.45}$$

which results in:

$$\Delta q_{i+1} = J\Delta q_i \tag{4.46}$$

where J is defined as:

$$J = \frac{\partial S}{\partial q} \mid_{q=q^*} \tag{4.47}$$

On the other hand, we have:

$$\Delta q_i = q_i - q^* \tag{4.48}$$

Afterward, based on Eqs. (4.46) and (4.48), we can conclude:

$$q_{i+1} - q_i = (J - I)\Delta q_i \tag{4.49}$$

where I is the identity matrix. Also, employing Eq. (4.34) leads to:

$$S(q_i) - q_i = (J - I)\Delta q_i \tag{4.50}$$

Next, a computer program could be written based on the following algorithm:

$$\begin{aligned} &Repeat \\ &\qquad \Delta q_i = (J - I)^{-1}(S(q_i) - q_i) \\ &\qquad q_i = q_i + \Delta q_i \\ &Until \ \mid \Delta q_i \mid < \varepsilon \end{aligned} \tag{4.51}$$

where ε is a small disturbance added to the system. Also, the Jacobian matrix, J, can be numerically calculated in every iteration. Now, if the algorithm is convergent, the fixed point and its corresponding Jacobian matrix simultaneously emerge. Otherwise, either the algorithm must be run again with a new initial guess or we need to change the system's parameters. Finding the first fixed point would help to find other fixed points in its vicinity. In this regard, a new initial guess is defined as a point near the found fixed point. Therefore, trial-and-error is merely necessary to reveal the first limit cycle.

To examine the stability, one also needs to calculate the largest absolute eigenvalue of J, i.e. $\mid \Lambda \mid_{max}$. For this conservative system, the minimum of $\mid \Lambda \mid_{max}$ would be 1. That means since the system is not dissipative, by passing time, a disturbing limit cycle remains perturbed, albeit it would be very close to the unperturbed trajectory. So stability is guaranteed, although walking is not asymptotically stable. If $\mid \Lambda \mid_{max} > 1$ the limit cycle and its corresponding fixed point are unstable. Note, in this case, it is feasible to take several successful steps without falling. We implemented the algorithm in MATLAB and used the 'ode45' function to solve the equations of motion numerically.

4.2 Collection of walking data

The experimental data is collected from walking of a healthy subject (111 kg weight, 185 cm height) on a treadmill for one hundred steps at five different speeds, ranging from 1.5 to 3.5 mph, in increments of 0.5 mph. This range definitely covers the slow, normal, and fast walking of the subject. It is obtained based on the self-selected, desired speed of the subject, followed by 20% and 40% slower and faster speeds. For data recording, the GRFs were measured by force plates at 1000 Hz, and the hip coordinates were sampled by VICON at 200 Hz. Unfortunately, due to a very high level of noise or completely useless data, we excluded data related to 1.5 mph from our analysis. Furthermore, to have a fair comparison among other speeds, we looked for the maximum number of

consecutive good strides that are common among all speeds. So, only 40 steps from different time intervals of different speeds were selected.

Noise is a part of the data, and especially is observed during measuring the GRFs. To make data smooth without losing any considerable information, we employed 'smoothdata' function in MATLAB, and applied it to the sequence of intervals through all data. These intervals are partitioned with the same size. We used 'sgolay' method (Savitzky-Golay filter). It smooths according to a quadratic polynomial that is fitted over each window of data. This method is more efficient than other existing methods when the data is too rugged and varies quickly.

4.3 Fitting DSLIP model to walking data

We want to assess DSLIP as a model for human walking by fitting it to the empirical data. In this regard, we employ two different strategies. First, we try to fit the model to each step separately. This gives us an individual non-periodic trajectory for each step that is not connected to the former and latter steps. Second, by averaging empirical data for each walking speed and using the optimized non-periodic trajectories, we try to fit a single limit cycle to all steps. Besides numerous insights about the nature of human walking and the abilities of the model, this procedure proposes a systematic approach to find an appropriate limit cycle in a simple and acceptable way.

4.3.1 Optimized non-periodic trajectories

Looking for a non-periodic trajectory means that we have more flexibility. In fact, since we remove the symmetry and limit cycle constraints, the number of independent parameters for the dimensionless system increases. Also here, instead of the definition of a step from a mid-stance to a mid-stance, we can suppose that a step begins with a single stance phase and finishes at the end of the double support phase. This replacement lets the system parameters vary after the toe-off event instead of the mid-stance, which is more reasonable. Note we used mid-stance as the Poincaré section just to simplify finding limit cycles and describing symmetric conditions. According to this new definition, the system parameters can be reset as follows:

$$P^{'} = \{\lambda, \gamma, \theta_0, \dot{\theta}_0, r_0, \dot{r}_0\} \tag{4.52}$$

where, θ_0, $\dot{\theta}_0$, r_0, and $\dot{r}_0$ are dimensionless angular position, angular velocity, radial displacement, and radial velocity of the new stance leg at the beginning of each step, respectively.

Furthermore, we are interested in fitting not only GRFs, but also the step length, speed, and position of CoM. To this end, we have to consider the model with full dimension, so R_{nat} must be defined as well. Moreover, because of the unknown location of CoM in the subject, we add a new parameter called D which defines the vertical distance between the hip and CoM. Note $D > 0$ means the CoM is over the hip.

Before doing optimization, we need to define R_{nat} and D; since these parameters are approximately constant and do not vary from one step to another. In this regard, we suppose the estimated D is within 10 cm from the measured vertical position of the hip at the mid-stance, and the amount of spring contraction at mid-stance is around %5; so we have:

$$107\,cm \leq R_{nat} \leq 128\,cm \tag{4.53}$$

Based on this inequality, we choose 4 different values for R_{nat} as 107, 114, 121, and 128 cm. Then the corresponding value of D can be calculated from:

$$R_{nat} = 1.05(D + H_h) \tag{4.54}$$

where H_h is the average height of the hip at the mid-stance. To determine other parameters, we need to do optimization. There are several ways to define a cost function. The more complex, the harder to find out the global minimum. So, to avoid local minimums as well as keep the important features of human walking, the optimization algorithm tries to minimize the errors related to the following items:

- The vGRF at mid-stance
- The peaks of vGRF
- The CoM height at mid-stance
- The single stance time
- The step time
- The step length

These seven most important characteristics would be easily possible to get minimized by optimizing the system's parameters. Note it is feasible to reduce the dimension of parameter space by fixing λ to the dimensionless step length of the subject, i.e. the step length divided by R_{nat}. Instead, we can calculate the error of the step length by subtracting the model's CoM horizontal displacement from the step length of the subject. This helps to get the optimized trajectory as symmetric as possible. Also since we try to minimize the error related to the step time, it means that we keep the speed of the model the same as the subject.

To do optimization, a computer program was written by using 'Global Optimization Toolbox' of MATLAB along with 'fmincon' function, 'sqp' algorithm, and 'MultiStart' object. We also determine the boundaries for our parameters as follows:

$$\begin{aligned} 5 \leq \gamma \leq 70 \\ 0.05 \leq \theta_0 \leq 0.50 \\ -0.50 \leq \dot{\theta}_0 \leq -0.05 \\ -0.15 \leq r_0 \leq 0 \\ -0.10 \leq \dot{r}_0 \leq 0.10 \end{aligned} \tag{4.55}$$

We did optimization for the specified values of R_{nat} and four different walking speeds, ranging from 2.0 mph to 3.5 mph, in increments of 0.5 mph. Then by employing root-mean-square error (RMSE), calculated for vGRF, hGRF, CoM height, and CoM horizontal displacement, we find the best value for R_{nat}. This single value is used to find the optimized limit cycle for each speed separately.

4.3.2 Optimized limit cycles

Since limit cycles describe a harmonic motion in a dynamical system, it is not meaningful to look for them for each step separately. In contrast, by considering human walking as a dynamical system, it is more acceptable to fit a single limit cycle to all steps. To this end, first, we are interested in using the information gained from the previously optimized trajectories as a basis. In this regard, the most important parameters that can be beneficial are R_{nat} and D. Thus, for the optimized limit cycles, R_{nat} and D are predefined and fixed. Also, λ is chosen based on the average step length of the subject for each speed divided by R_{nat}. The next parameter is selected as the subject average speed in its modified form called Froude number, Fr, which is calculated according to the following equation:

$$Fr = \frac{V_{trd}^2}{R_{nat} g} \tag{4.56}$$

where, V_{trd} is the treadmill speed. There is merely one left parameter that must be determined to have a full dimension limit cycle, emulating the GRFs and CoM's trajectory of the subject. Here, we choose the dimensionless form of vGRF at the mid-stance (the minimum vGRF of the subject during the single stance phase divided by the weight of the subject), $\gamma\delta_0$, since it is available from the data. The other choice could be the single stance time; however because we have already kept the step length and the speed of the subject, the period of the cycle is fixed. So instead of tracking another kinematic variable, it would be better to try to fit something from the force diagram. Now, by plotting the solution space for the fixed λ and in Fr-$\gamma\delta_0$ plane, we can choose the limit cycle which has the same λ and Fr as the subject and has the closest location to the empirical data according to the minimum vGRF during the single stance phase. Beyond its simplicity, this is an effective method to judge the model and its ability to predict empirical data.

Acknowledgements: T.B. was funded by the Howard Hughes Medical Institute. This research was supported by RO1DC015827 (VB), RO1NS097881 (VB) and an NSF CAREER award (IOS-1652647 to VB).

References

Adamczyk, P. G. and Kuo, A. D. (2009). Redirection of center-of-mass velocity during the step-to-step transition of human walking. *Journal of Experimental Biology*, 212(16):2668–2678.

Ahn, A. N., Furrow, E., and Biewener, A. A. (2004). Walking and running in the red-legged running frog, kassina maculata. *Journal of Experimental Biology*, 207(3):399–410.

Andrada, E., Blickhan, R., Ogihara, N., and Rode, C. (2020). Low leg compliance permits grounded running at speeds where the inverted pendulum model gets airborne. *Journal of Theoretical Biology*, 494:110227.

Andrada, E., Nyakatura, J. A., Bergmann, F., and Blickhan, R. (2013a). Adjustments of global and local hindlimb properties during terrestrial locomotion of the common quail (coturnix coturnix). *Journal of Experimental Biology*, 216(20):3906–3916.

Andrada, E., Rode, C., and Blickhan, R. (2013b). Grounded running in quails: simulations indicate benefits of observed fixed aperture angle between legs before touch-down. *Journal of theoretical biology*, 335:97–107.

Andrada, E., Rode, C., Sutedja, Y., Nyakatura, J. A., and Blickhan, R. (2014). Trunk orientation causes asymmetries in leg function in small bird terrestrial locomotion. *Proceedings of the Royal Society B: Biological Sciences*, 281(1797):20141405.

Antoniak, G., Biswas, T., Cortes, N., Sikdar, S., Chun, C., and Bhandawat, V. (2019). Spring-loaded inverted pendulum goes through two contraction-extension cycles during the single-support phase of walking. *Biology open*, 8(6):bio043695.

Basu, C., Wilson, A. M., and Hutchinson, J. R. (2019). The locomotor kinematics and ground reaction forces of walking giraffes. *Journal of Experimental Biology*, 222(2):jeb159277.

Biswas, T., Rao, S., and Bhandawat, V. (2018). A simple extension of inverted pendulum template to explain features of slow walking. *Journal of theoretical biology*, 457:112–123.

Blickhan, R. (1989). The spring-mass model for running and hopping. *Journal of biomechanics*, 22(11-12):1217–1227.

Blickhan, R., Andrada, E., Hirasaki, E., and Ogihara, N. (2018). Global dynamics of bipedal macaques during grounded and aerial running. *Journal of Experimental Biology*, 221(24):jeb178897.

Blickhan, R. and Full, R. (1993). Similarity in multilegged locomotion: bouncing like a monopode. *Journal of Comparative Physiology A*, 173:509–517.

Bonnaerens, S., Fiers, P., Galle, S., Aerts, P., Frederick, E. C., Kaneko, Y., Derave, W., et al. (2019). Grounded running reduces musculoskeletal loading. *Medicine and Science in Sports and Exercise*, 51(4):708–715.

Buczek, F. L., Cooney, K. M., Walker, M. R., Rainbow, M. J., Concha, M. C., and Sanders, J. O. (2006). Performance of an inverted pendulum model directly applied to normal human gait. *Clinical Biomechanics*, 21(3):288–296.

Daley, M. A., Felix, G., and Biewener, A. A. (2007). Running stability is enhanced by a proximo-distal gradient in joint neuromechanical control. *Journal of Experimental Biology*, 210(3):383–394.

Davis, S., Fox, A., Bonacci, J., and Davis, F. (2020). Mechanics, energetics and implementation of grounded running technique: a narrative review. *BMJ Open Sport & Exercise Medicine*, 6(1):e000963.

Ding, J., Moore, T. Y., and Gan, Z. (2022). A template model explains jerboa gait transitions across a broad range of speeds. *Frontiers in Bioengineering and Biotechnology*, 10.

Donelan, J. M., Kram, R., and Kuo, A. D. (2002). Mechanical work for step-to-step transitions is a major determinant of the metabolic cost of human walking. *Journal of experimental biology*, 205(23):3717–3727.

Farley, C. T. and Gonzalez, O. (1996). Leg stiffness and stride frequency in human running. *Journal of biomechanics*, 29(2):181–186.

Gan, Z., Yesilevskiy, Y., Zaytsev, P., and Remy, C. D. (2018). All common bipedal gaits emerge from a single passive model. *Journal of The Royal Society Interface*, 15(146):20180455.

Geyer, H. (2005). *Simple models of legged locomotion based on compliant limb behavior*. PhD thesis.

Geyer, H., Seyfarth, A., and Blickhan, R. (2006). Compliant leg behaviour explains basic dynamics of walking and running. *Proceedings of the Royal Society B: Biological Sciences*, 273(1603):2861–2867.

Griffin, T. M., Main, R. P., and Farley, C. T. (2004). Biomechanics of quadrupedal walking: how do four-legged animals achieve inverted pendulum-like movements? *Journal of Experimental Biology*, 207(20):3545–3558.

Hubel, T. Y. and Usherwood, J. R. (2015). Children and adults minimise activated muscle volume by selecting gait parameters that balance gross mechanical power and work demands. *Journal of Experimental Biology*, 218(18):2830–2839.

Kim, S. and Park, S. (2011). Leg stiffness increases with speed to modulate gait frequency and propulsion energy. *Journal of biomechanics*, 44(7):1253–1258.

Kram, R., Domingo, A., and Ferris, D. P. (1997). Effect of reduced gravity on the preferred walk-run transition speed. *The Journal of experimental biology*, 200(4):821–826.

Kuo, A. D. (2001). A simple model of bipedal walking predicts the preferred speed–step length relationship. *J. Biomech. Eng.*, 123(3):264–269.

Kuo, A. D. (2002). Energetics of actively powered locomotion using the simplest walking model. *J. Biomech. Eng.*, 124(1):113–120.

Kuo, A. D., Donelan, J. M., and Ruina, A. (2005). Energetic consequences of walking like an inverted pendulum: step-to-step transitions. *Exercise and sport sciences reviews*, 33(2):88–97.

Lee, C. R. and Farley, C. T. (1998). Determinants of the center of mass trajectory in human walking and running. *Journal of experimental biology*, 201(21):2935–2944.

Lim, H. and Park, S. (2019). A bipedal compliant walking model generates periodic gait cycles with realistic swing dynamics. *Journal of Biomechanics*, 91:79–84.

Lin, B., Živanović, S., Zhang, S., Zhang, Q., and Fan, F. (2023). Evaluation of compliant walking locomotion models for civil engineering applications. *Journal of Sound and Vibration*, 561:117815.

Lipfert, S. W., Günther, M., Renjewski, D., Grimmer, S., and Seyfarth, A. (2012). A model-experiment comparison of system dynamics for human walking and running. *Journal of theoretical biology*, 292:11–17.

Mauersberger, M., Hähnel, F., Wolf, K., Markmiller, J. F., Knorr, A., Krumm, D., and Odenwald, S. (2022). Predicting ground reaction forces of human gait using a simple bipedal spring-mass model. *Royal Society Open Science*, 9(7):211582.

Maus, H.-M., Lipfert, S., Gross, M., Rummel, J., and Seyfarth, A. (2010). Upright human gait did not provide a major mechanical challenge for our ancestors. *Nature communications*, 1(1):70.

Maus, H.-M., Revzen, S., Guckenheimer, J., Ludwig, C., Reger, J., and Seyfarth, A. (2015). Constructing predictive models of human running. *Journal of The Royal Society Interface*, 12(103):20140899.

McMahon, T. A. and Cheng, G. C. (1990). The mechanics of running: how does stiffness couple with speed? *Journal of biomechanics*, 23:65–78.

Müller, R., Rode, C., Aminiaghdam, S., Vielemeyer, J., and Blickhan, R. (2017). Force direction patterns promote whole body stability even in hip-flexed walking, but not upper body stability in human upright walking. *Proceedings of the Royal Society A: Mathematical, Physical and Engineering Sciences*, 473(2207):20170404.

Nishikawa, K., Biewener, A. A., Aerts, P., Ahn, A. N., Chiel, H. J., Daley, M. A., Daniel, T. L., Full, R. J., Hale, M. E., Hedrick, T. L., et al. (2007). Neuromechanics: an integrative approach for understanding motor control. *Integrative and comparative biology*, 47(1):16–54.

Reinhardt, L. and Blickhan, R. (2014). Level locomotion in wood ants: evidence for grounded running. *Journal of Experimental Biology*, 217(13):2358–2370.

Rummel, J., Blum, Y., and Seyfarth, A. (2010). Robust and efficient walking with spring-like legs. *Bioinspiration & biomimetics*, 5(4):046004.

Schmitt, D. (1999). Compliant walking in primates. *Journal of Zoology*, 248(2):149–160.

Shorten, M. and Pisciotta, E. (2017). Running biomechanics: what did we miss? *ISBS Proceedings Archive*, 35(1):293.

Srinivasan, M. (2011). Fifteen observations on the structure of energy-minimizing gaits in many simple biped models. *Journal of The Royal Society Interface*, 8(54):74–98.

Srinivasan, M. and Ruina, A. (2006). Computer optimization of a minimal biped model discovers walking and running. *Nature*, 439(7072):72–75.

Usherwood, J. R. (2005). Why not walk faster? *Biology letters*, 1(3):338–341.

Whittington, B. R. and Thelen, D. G. (2009). A simple mass-spring model with roller feet can induce the ground reactions observed in human walking. *Journal of Biomechanical Engineering*, 131(1).

Wisse, M., Schwab, A. L., and van der Helm, F. C. (2004). Passive dynamic walking model with upper body. *Robotica*, 22(6):681–688.

Supplementary Materials

A Single stance dynamics and different gait patterns

Let us characterize the different gaits DSLIP can realize that, at most, exhibit a single radial (leg length) oscillation. We can write the equations of motion for the single stance phase in dimensionless polar coordinates (Table 1) centered around the point of ground contact as

$$\ddot{\delta} = -(1-\delta)\dot{\theta}^2 - \gamma\delta + \cos\theta \tag{A.1}$$

$$\ddot{\theta} = (\sin\theta + 2\dot{\delta}\dot{\theta})/(1-\delta) \ . \tag{A.2}$$

where δ represents the dimensionless spring contraction, and θ defines the angular coordinate.

For the most part we are going to consider symmetric limit cycles. This means that at the mid-stance the CoM either has a minimum or a maximum in kinematic variables such as vertical height, and vGRF. We will show that three different gaits are possible depending upon the height and vGRF profiles with at most a single radial (leg length) oscillation. The normal gait has a height maximum and vGRF minimum at mid-stance, while both the inverted gaits (grounded running and inverted walking) have a vGRF maximum at mid-stance. While the grounded running has a height minimum at mid-stance, inverted walking has a height maximum similar to normal walking gait. Finally, let us reiterate (Biswas et al., 2018) that within the DSLIP model there is no provision to have a mid-stance maximum in horizontal velocity, it always has a minimum. The different gait characteristics are summarized in the table below along with the relationships between gait parameters that must be satisfied. We now derive these relationships.

To ascertain the region in parameter space where the different gaits emerge, first consider the vertical acceleration at the mid-stance:

$$\ddot{h}_0 = \gamma\delta_0 - 1 \ . \tag{A.3}$$

Clearly then to have a maximum in height we must have $\delta_0 < 1/\gamma$. Now the vertical spring force is given by

$$\bar{F}_y = \gamma\delta\cos\theta \ . \tag{A.4}$$

Using (A.2) we find that at the mid-stance

$$\ddot{\bar{F}}_y = \gamma[1 - \gamma\delta_0 - \Omega_0^2] \ . \tag{A.5}$$

For $\bar{F}_y$ to have a minimum at the mid-stance then, this must be positive, or

$$\delta_0 \leq \frac{1-\Omega_0^2}{\gamma} \ . \tag{A.6}$$

We also note that for a given λ there is an upperbound for δ_0 to have any single stance phase at all, see Fig.?:

$$\delta_0 < 1 - \sqrt{1-\lambda^2} \equiv \delta_{\max} \ . \tag{A.7}$$

Thus based on the range of δ_0 one can have different gait profiles that we tabulate below:

gait	mid-stance height	mid-step height	mid-stance vGRF	mid-step vGRF	mid-stance velocity	δ_0 range
normal walk	maximum	minimum	minimum	maximum	minimum	$0 < \delta_0 < \frac{1-\Omega_0^2}{\gamma}$
inverted walk	maximum	minimum	maximum	minimum	minimum	$\frac{1-\Omega_0^2}{\gamma} < \delta_0 < \frac{1}{\gamma}$
grounded run	minimum	maximum	maximum	minimum	minimum	$\frac{1}{\gamma} < \delta_0$

B Approximate Trajectories

Our goal in this subsection is to derive approximate trajectories of the CoM in order to gain analytical insights into how different parameters must adjust to have a synchronized motion. Also, this will help us address how well DSLIP is able to capture some of the well-known features of the walking gait.

B.1 Single stance phase

Starting from the dynamical equations in polar coordinates (A.1, A.2), solutions for $\delta(t)$ and $\phi(t)$ were derived in the main manuscript,

$$\begin{aligned} \delta &= \frac{1}{\gamma} + \left(\delta_0 - \frac{1}{\gamma}\right)\cos(\omega t) \\ \theta &= \Omega_0 t \end{aligned} \tag{B.1}$$

where we assumed that the angular and radial motion during the single stance phase are effectively decoupled. The main idea behind this approximation is that for walking trajectories the radial motion undergoes oscillations around its equilibrium position $\delta_{eq} = 1/\gamma$, and since $\gamma \sim \mathcal{O}(10) - \mathcal{O}(100)$, the oscillations are small. We also assume that the angular/horizontal velocity of CoM remains approximately constant. Technically, this means that we are ignoring $\dot{\theta}^2$ term as compared to $(\gamma\delta)$ in (A.1). Since $\dot{\theta}^2 \sim \Omega_0^2$ and $(\gamma\delta) \sim 1$ on an average, this boils down to assuming $\dot{\theta}^2 \ll 1$ which is valid for the speeds we are interested in. We also assume that $\dot{\theta}$ is approximately constant, or $\ddot{\theta} \approx 0$. By inspection of (A.2) $\ddot{\theta}$ depends on θ but this is small, $\theta < \lambda/2$, for the steplengths under consideration. $\ddot{\theta}$ also depends on $(\dot{\delta}\dot{\theta})$. While $\dot{\theta} \sim \Omega_0 < 1$, on an average $\dot{\delta}$ is close to zero suggesting a small effect coming from this term $(\dot{\delta}\dot{\theta})$. We shall see, that these approximations provide valuable qualitative and quantitative insights into the dynamics and the relationship between various relevant dynamical parameters.

B.2 Transition to double stance

As argued in the main manuscript, synchronization between the radial and angular motion relates γ and Ω_0 as

$$\Omega_0 = \left(\frac{\theta_\star}{\phi_\star}\right)\sqrt{\gamma}\ , \tag{B.2}$$

where $\star$ marks the values at the transition point between the single and double stance phases. From geometry, we can find $\theta_\star$ as

$$\sin\theta_\star = \frac{\lambda^2 + (1-\delta_\star)^2 - 1}{2(1-\delta_\star)\lambda} \tag{B.3}$$

while substituting $\delta = \delta_\star$, and $\omega t = \phi_\star$ in (B.1) yields

$$\cos\phi_\star = -\left(\frac{\gamma\delta_\star - 1}{1-\gamma\delta_0}\right)\ . \tag{B.4}$$

The dependence of $\theta_\star, \phi_\star$ as a function of $\delta_\star$ are plotted in Figure 4B. In principle, the transition time can be found by solving

$$\lambda^2 + [1-\delta(t_\star)]^2 - 2[1-\delta(t_\star)]\lambda\sin\theta(t_\star) = 1\ . \tag{B.5}$$

so that $t_\star = t_\star(\lambda, \Omega_0, \gamma, \delta_0)$. One can then evaluate $\theta_\star = \theta(t_\star)$, and $\delta_\star = \delta(t_\star)$, to obtain the position of CoM at the transition, as well as the phase angle, $\phi_\star = \omega t_\star$. Thus all these quantities can be thought of as functions of four gait parameters, $\lambda, \Omega_0, \gamma$, and δ_0.

B.3 Double stance phase

To approximate the double stance phase we are going to assume that the horizontal velocity and the vertical acceleration remain approximately constant. The intuition behind these approximations is as follows: the two springy legs provide horizontal forces in opposing directions so that we expect the average horizontal acceleration to be small and therefore the horizontal velocity to remain approximately constant. Realistic walking trajectories typically exhibit low-velocity changes which further strengthens this argument, and we compute the horizontal velocity at the start of the double stance. In contrast with the horizontal motion where the legs oppose each other, both legs provide a vertically upward forces. At the beginning of the double stance phase, all the force comes from the leg that was supporting the single stance phase at the touchdown, the swing leg is at its natural length. Thereafter, while the initial stance leg unloads, the leg that touched down loads. Therefore we conjectured that the net upward force may not change much, and approximate the net force as a constant. The approximate trajectories in the double stance phase are thus given by

$$\begin{aligned} x(t) &= (1-\delta_\star)\cos\theta_\star + v_{x\star}(t-t_\star) \ , \\ y(t) &= (1-\delta_\star)\sin\theta_\star + v_{y\star}(t-t_\star) + \frac{1}{2}a_{y\star}(t-t_\star)^2 \ . \end{aligned} \tag{B.6}$$

where $v_{x\star}, v_{y\star}$, and $a_{y\star}$ can be calculated at the transition time as follows:

$$\begin{aligned} v_{x\star} &= (1-\delta_\star)\Omega_0\cos\theta_\star \ , \\ v_{y\star} &= -(1-\delta_\star)\Omega_0\sin\theta_\star \ , \\ a_{y\star} &= F_{y\star} = \gamma\delta_\star\cos\theta_\star - 1 \ . \end{aligned} \tag{B.7}$$

The ultimate test of these approximations, of course, will obviously be provided by comparing it with results from numerical simulation.

To summarize, Eqs. (2.5, B.5, B.6, B.7) together completely specifies a walking trajectory as a function of $\lambda, \Omega_0, \gamma$, and δ_0. We are now going to see how to maintain a steady limit cycle gait these four parameters must obey a specific relationship that can be derived by looking at the synchronization of the periodic angular and radial motion. We will also see how different gait patterns emerge.

C Limit cycles

C.1 Constraint from periodicity and synchronization

A key requirement of a sustainable walking gait is that after a given step the CoM returns to the same vertical height as the beginning of the cycle and also has the same velocity. Technically, the gait cycle should be a limit cycle. This is a technical way of ensuring that the different types of motion an animal undergoes are periodic and synchronized. For instance, in the context of the CoM motion, the vertical and horizontal motion have to be synchronized and this imposes important relationships between the parameters governing the dynamics, as we shall now see.

We will be able to derive this relationship by imposing that the time to reach the appropriate vertical and horizontal mid-step configuration that can be computed separately from the vertical and horizontal motion respectively, must be the same. For a limit cycle Using (B.6) we can calculate half of the horizontal distance traveled during the double stance:

$$x_d = \lambda/2 - (1-\delta_\star)\sin\theta_\star \ , \tag{C.1}$$

So, the half-time of the double stance phase is

$$\frac{1}{2}\tau_d = \frac{x_d}{v_x} = \frac{\lambda/2 - (1-\delta_\star)\sin\theta_\star}{(1-\delta_\star)\Omega_\star\cos\theta_\star} \ , \tag{C.2}$$

Now, due to the symmetry assumption, the vertical velocity is zero in the middle of the double stance phase. Therefore, it is possible to calculate t_d from the vertical kinematics as well

$$\frac{1}{2}\tau_d = \frac{\Delta v_y}{a_y} = \frac{0 - v_y}{a_y} = \frac{(1-\delta_\star)\Omega_\star \sin\theta_\star}{\gamma\delta_\star\cos\theta_\star - 1} \ , \tag{C.3}$$

Therefore, from (C.2) and (C.3) we can conclude

$$\Omega_\star^2 = \frac{(\gamma\delta_\star\cos\theta_\star - 1)(\lambda/2 - (1-\delta_\star)\sin\theta_\star)}{(1-\delta_\star)^2\sin\theta_\star\cos\theta_\star} \ , \tag{C.4}$$

Since we suppose that the angular velocity is approximately constant during the single stance phase, we can rewrite it as

$$\Omega_0^2 = \frac{(\gamma\delta_\star\cos\theta_\star - 1)(\lambda/2 - (1-\delta_\star)\sin\theta_\star)}{(1-\delta_\star)^2\sin\theta_\star\cos\theta_\star} \equiv G_D(\delta_0, \delta_\star, \gamma, \lambda) \ , \tag{C.5}$$

Moreover, from (2.9) we have

$$\Omega_0^2 = \left(\frac{\theta_\star}{\phi_\star}\right)^2 \gamma \equiv G_S(\delta_0, \delta_\star, \gamma, \lambda) \ . \tag{C.6}$$

Thus, in order to have a synchronized limit cycle the four parameters, $\delta_0, \delta_\star, \gamma, \lambda$ must be related:

$$G_D(\delta_0, \delta_\star, \gamma, \lambda) = G_S(\delta_0, \delta_\star, \gamma, \lambda) \ . \tag{C.7}$$

This explicitly demonstrates why all limit cycles can be characterized by only three parameters, for instance by $\delta_0, \gamma, \lambda$, as Ω_0 and $\delta_\star$ can be obtained via (C.6) and (C.7).

C.2 Different oscillatory mode solutions arise from the single stance phase constraint

In this subsection we will see how the gait parameter space of periodic (limit cycle) walking separates into different regions with different characteristic features. The different gaits fundamentally arise because $\delta(t)$ is a periodic function. Technically, one can see its effect in the multivalued nature of $\phi_\star$ as a function of γ, δ_0 and $\delta_\star$ as inferred from (B.4) using the cosine inverse. This in turn makes G_S a multivalued function and choosing different branches while solving (C.7) leads to different oscillatory limit cycle gaits. To understand this more intuitively suppose one wants to travel at a given speed (approximately fixing Ω_0) and a given step-length (λ). What the oscillatory evolution of $\delta(t)$ suggests is that even if one fixes the mid-stance contraction (δ_0), there may be more than one way to achieve synchronization needed for limit cycle walking. For instance consider the single stance synchronization condition (C.6): One can maintain approximately the same Ω_0, with the same transition angle [3], $\theta_\star$, either by choosing a relatively lower value of γ and oscillating less (smaller $\phi_\star$), or have a much higher γ and oscillate more ($\phi_\star$ approximately larger by a multiple of 2π). To ensure that the upward velocity can be reversed during the double stance phase, the trajectory with the smaller γ does require a little longer double stance time as compared to the larger γ trajectory. So, the transition must occur a little earlier in the lower oscillatory mode, and accordingly $t_\star, \delta_\star$, and $\theta_\star$, are not exactly the same for the two trajectories. However, the flexibility of undergoing different phases of oscillation approximately separated by multiples of 2π explains how the gait parameter space separates into different oscillatory gaits, and why even with the same λ, Ω_0 and δ_0, different γ and correspondingly different oscillatory modes are possible.

[3] In other words, achieve approximately the same contraction length, $\delta_\star$, approximately at the same same time, $t_\star$.

D Approximate speed range for different oscillatory gaits

In this section, we provide a technical discussion on why the different oscillatory gaits are associated with different speed ranges. We specifically demonstrate why it is not possible to walk too fast in the normal walking gait.

D.1 Inverted and grounded running can lead to high walking-speeds.

We will first discuss the inverted walking gait whose CoM trajectory resembles that of the normal walking gait but has a different vGRF profile. We will show that while it is subjected to a lower bound in speed, one can theoretically walk much faster using this gait as compared to the normal walking gait. To see this, let us remind ourselves that for inverted walking approximately we have, $0 < \phi_\star < \frac{\pi}{2}$. According to (C.6), for a fixed γ one can decrease the speed by increasing $\phi_\star$, but since the latter has an upperbound leading we have

$$\Omega^2_{0,\min} = \left(\frac{2\theta_\star}{\pi}\right)^2 \gamma \ , \tag{D.1}$$

where approximately $\theta_\star$ should be calculated by substituting $\delta_\star = \delta_{eq} = 1/\gamma$ consistent with $\phi_\star = \pi/2$. Incidentally, this coincides with the upperbound for normal walking, see also Fig.?. In contrast to having a lower bound in speed for a fixed γ, by decreasing $\phi_\star$ all the way to zero, the speed can be increased arbitrarily according to the single stance constraint (C.6). Just as in the normal walking gait though, the velocity redirection constraint coming from double stance phase limits the maximum speed attainable and this bound agrees well with our numerical simulation. Nevertheless, $\phi_\star$ can be much smaller in the inverted walking gait in comparison with the range available for normal walking gait, and therefore much larger speeds can be accessed in this gait as compared to the normal walking gait.

Let us next focus on the grounded running gait. In contrast to all other gaits the grounded running gait has an inverted CoM trajectory where in between the mid-stance and mid-step during the single stance phase, the CoM has a vertically upward velocity. This obviates the need to have an upward force during the double stance phase in order to redirect the velocity. This means that we should no longer require $\delta_\star > \delta_{eq} = 1/\gamma$. So, $\phi_\star$ need not satisfy, $0 < \phi_\star < \frac{\pi}{2}$, but could be larger, as borne out bt our simulations. More importantly, it is clear that in the grounded running gait, the radial velocity can no longer be ignored as compared to the angular velocity, in fact, the upward component of the radial velocity dominates over the downward component associated with the angular motion. Thus our estimate of the transition velocity (B.7), which was essentially based on angular motion, can no longer be trusted, and the limit cycle constraint (C.7) which gave rise to the maximum speed-bound in other gaits, is no longer valid. Surprisingly though our analytical estimates for such gaits continue to be broadly consistent with the numerical simulations, see Fig.?. Intuitively, high speeds in normal walking gait became impossible to attain because the upward force had a maximum and the time it had in the double stance phase shrunk with increasing speed eventually making it impossible to redirect the vertical velocity. Grounded running is this very special gait where the velocity in the single stance phase after the mid-step is upward and hence there is no need for velocity redirection. Thus the speed maximum constraint coming from velocity redirection is not applicable, and indeed in our numerical simulations we see the grounded running gait to be able to access larger and larger speeds by increasing γ.

D.2 Normal walking is bounded by the double stance phase constraint

For normal walking we have shown that $\frac{\pi}{2} < \phi_\star < \frac{3\pi}{2}$. Moreover, we know that by varying $\delta_\star$, $\theta_\star$ does not change too much (see Figure 4B). So according to (C.6), again we have two options

to increase the speed. Decreasing $\phi_\star$ and increasing γ. However, in contrast to grounded running, there is a conflict between these two options for normal walking. In summary, for high speeds, if $\phi_\star$ decreases as much as possible, we have $\phi_\star \longrightarrow \frac{\pi}{2}$, that leads to $\gamma\delta_\star \longrightarrow 1$; so the force might not be enough to redirect the CoM velocity during double stance phase. In other words, the increase in speed needs an increase in transition force; and to have the maximum transition force we must have $\gamma\delta_\star \longrightarrow 2$, which leads to $\phi_\star \longrightarrow \pi$. So at the upper bound of speed, to satisfy both constraints from single and double support phases ((C.5) and (C.6)), $\phi_\star$ settles somewhere between $\frac{\pi}{2}$ and π. On the other hand, there is only a little effect of the double stance constraint on the lower bound of speed (see Figure 5G and S**??**). This boundary deviation from the single stance constraint can be observed better for high values of γ in which the need for higher force increases. For the lower bound, although $\phi_\star$ is somewhere between $\frac{3\pi}{2}$ and π, it is much closer to $\frac{3\pi}{2}$ rather than π.

D.3 Slow walking via multiple oscillation modes

According to (C.6), by increasing $\phi_\star$ over the normal walking range, it is quite possible to jump to the slow walking region. In this situation, since there is no concern about the speed-force relationship, the double stance constraint does not play the main role again.

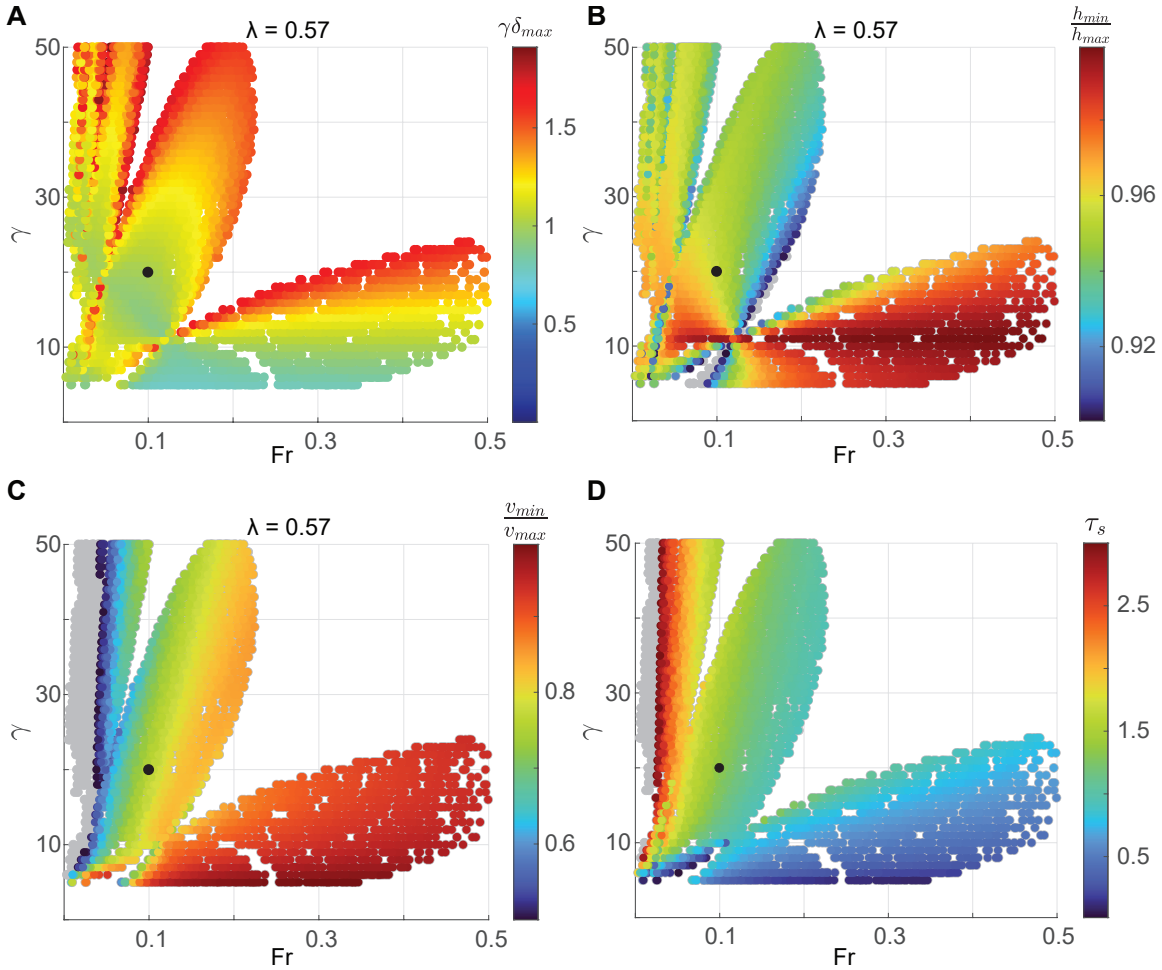

Figure S1. How important dynamic and kinematical features vary across gaits. A. We show how the maximal force, $\gamma\delta_{\max}$, exterted during a gait cycle varies across limit cycles. We note that lower the number of oscillations the lower is the maximal force required.In **B.** and **C.** We assess how the height and horizontal speed varies during a gait cycle by calculating the ratio between their maximum and minimum values, $h_{\min}/h_{\max}$, and $v_{\min}/v_{\max}$ respectively. We note that while the variations in the normal gait lies mostly within the ranges observed in humans, the higher oscillatory gaits show a larger variation in speed. **D.** Here we depict how the single-stance or swing time varies across different gait cycles. We see that cycles more number of oscillations have a longer time and therefore lower frequency. Since energy loss due to swing increases with higher frequency, this suggests that high oscillatory modes are energetically preferred. In all these figures the black dot represents the limit cycle that best fits experimental walking data at 2 miles/hour. We note that it exhibits relatively small variation in speed and height. Moreover, as compared to inverted gait cycles (at the same speed) it expends less swing energy, and as compared to higher oscillatory modes exerts less force. In concert, these plots argue why the normal gait is the preferred gait.

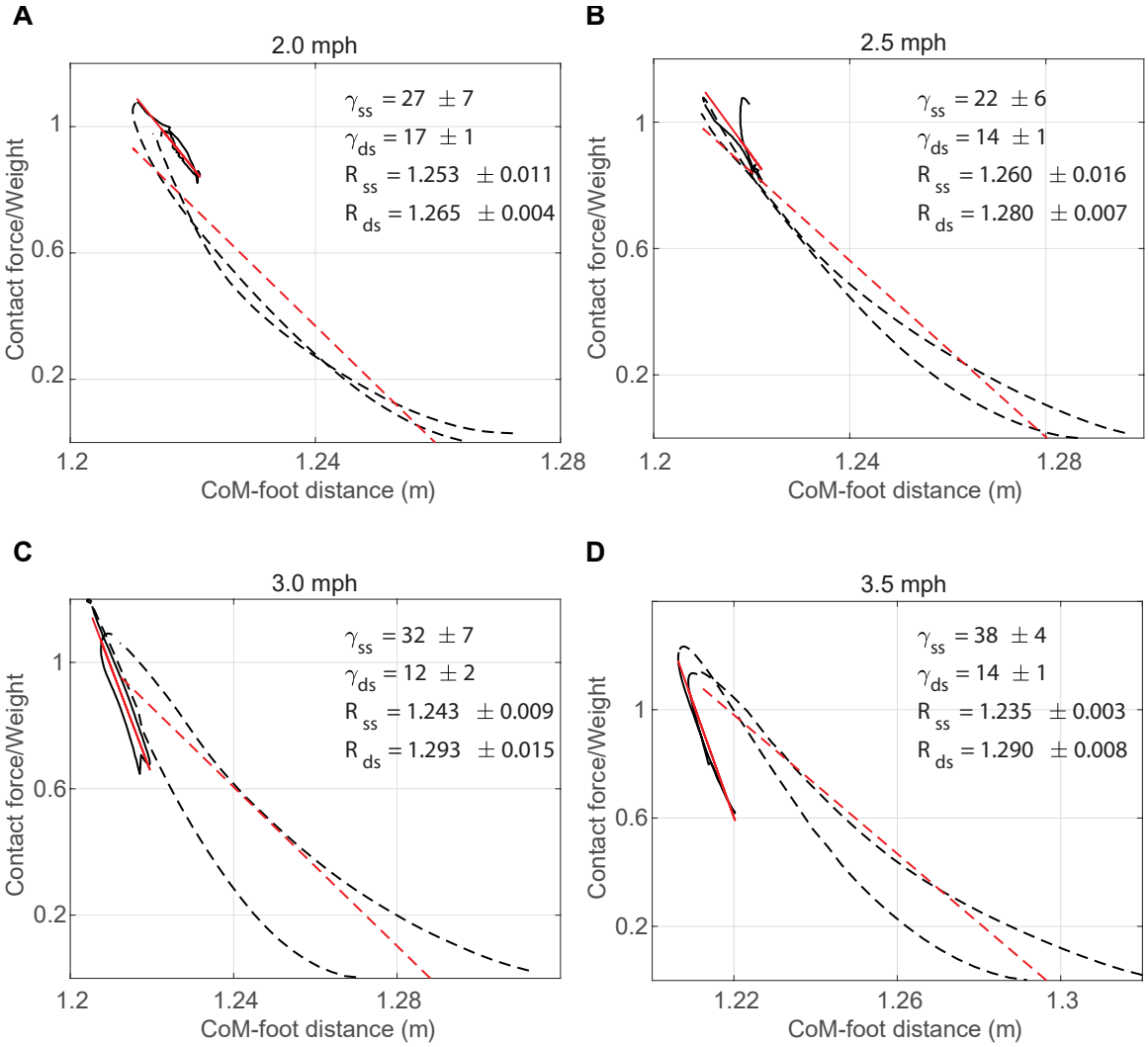

Figure S2. Force-length relationship shows that except for walking at 2.5 mph, the spring constants during single and double stance phases are different Each panel shows the force-length relationship for a single step. Dotted black line is during the single support phase, and solid black lines are during the double support phase. Red dotted and solid line show the best fitting linear spring to the single and double support phases. The mean and the SD of the spring constants and natural leg length are also reported for each speed.

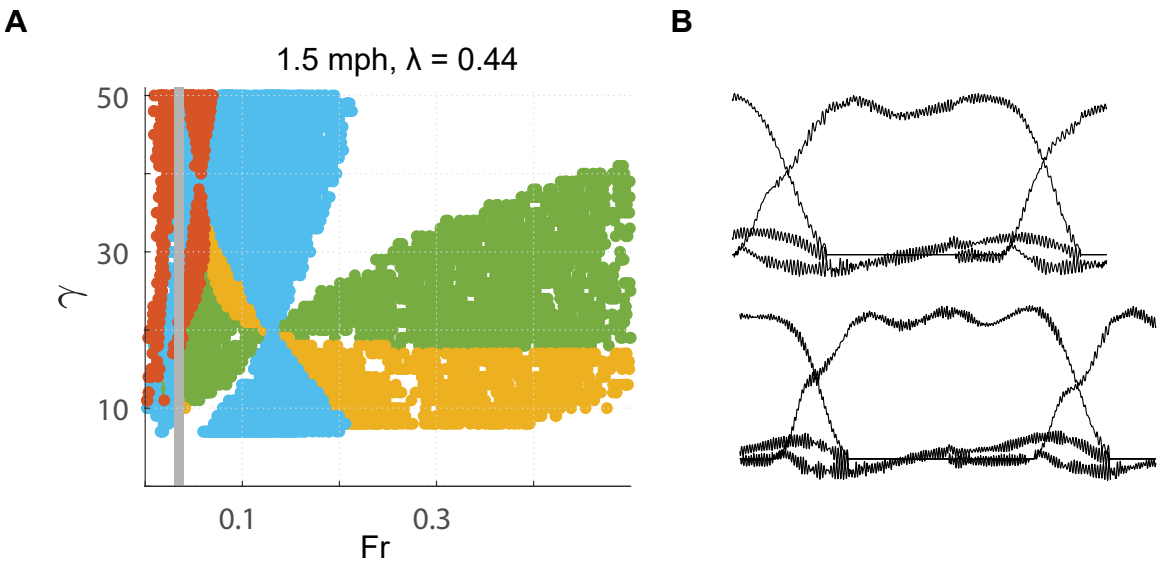

Figure S3. Human walking can involve higher oscillatory modes at low speed . A. At low speeds, such as, at a Fr number of 0.04 (gray line), both an M-shaped GRF (blue), and higher oscillation mode (orange) are possible. **B**. vGRF at these walking speeds can show both an M-shaped GRF, and GRF with higher number of oscillation as seen by the three-humped vGRF pattern.

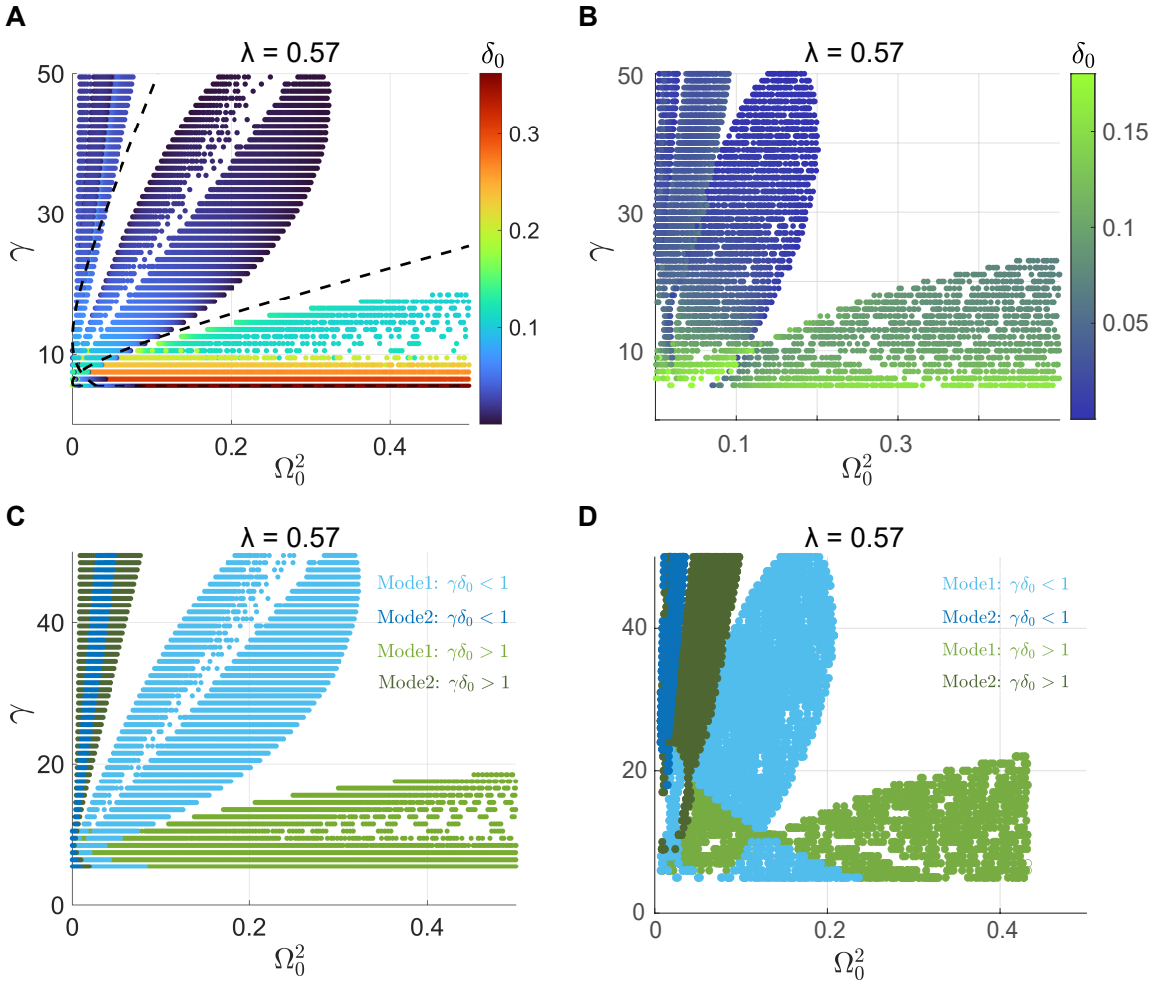

Figure S4. Comparison between analytically and numerically obtained limit cycles. A. We show the analytical solutions for a fixed step-length that are characterized by three quantities: the x-axis and y-axis corresponds to Ω_0^2 and γ respectively, while the color represents the value of δ_0. **B.** To compare with the analytical results we here depict numerical limit cycle solutions using the same color axis scale to represent δ_0 values. The analytical and numerical plots show similar patterns, and while the analytical solution over-estimates the value of δ_0, its variation both along the Ω_0^2-axis and γ-axis show similar trend as the numerical plot. **C.** and **D.** shows the same plots as **A.** and **B.** respectively, except that the color now represents the identity of the gait, normal, inverted or exhibiting multiple oscillations. While there are some discrepancies between the analytical and numerical results, they are broadly consistent with each other.